Optimization of growth and imaging techniques for *Medicago truncatula* and investigation of root hair nuclear positioning during early rhizobial infection

Undergraduate Research Thesis

Presented in Partial Fulfillment of the Requirements for graduation "with Honors Research Distinction" in the undergraduate colleges of The Ohio State University

by
Katherine Beigel

The Ohio State University
April 2017

Project Advisor: Dr. Iris Meier, Department of Molecular Genetics

TABLE OF CONTENTS

SECTION PAGE NUMBER

Table of Contents 1
Abstract 2
Introduction 3
Objectives 4
Results 7
Discussion 21
Materials & Methods 25
Acknowledgements 29
References 29

ABSTRACT

Legumes establish mutualistic relationships with endosymbiotic nitrogen-fixing rhizobia, which develop and dwell within nodules at the plant's roots. Rhizobia present in the legume's edaphic environment respond to compounds secreted by the plant with Nodulation (Nod) factors. The legume's root hair tips swell in response to these Nod factors, followed by additional cellular changes of the root hair that eventually coordinate infection thread (IT) formation, including curling of the root hair tip around a rhizobium. One of the suspected changes in the initial stages of nodulation is the movement of the root hair nucleus to the root hair tip around the time of root hair curling, based on anecdotal observations of the nucleus at the root hair tip after curing has completed. This positioning may indicate tip growth, and it has also been shown that the path of the IT down the root hair follows behind the nucleus. However, the details and subtleties of nuclear movement in the stages prior to IT formation are not well characterized.

Using a stable *Medicago truncatula* (Fabaceae) nuclear localized cameleon Ca^{2+} reporter line (YC3.6) and a dsRed-labeled *Sinorhizobium melliloti* rhizobia strain, I refined a methodology for observing root hairs and their nuclei. I tested and adapted growth, infection, and imaging methods from previous literature to establish a protocol for making observations with these two particular lines. I identified open source software for making observations and collecting data from confocal images.

With this protocol, seedlings of *M. truncatula* were monitored and imaged using z-stacks every 24 hours for five days after time of inoculation using live on-plate imaging techniques and confocal fluorescence microscopy. The root hairs imaged were those in the maturation zone just above the elongation zone. Measurements were made of the distance between the nucleus and the base, the distance between the nucleus and the tip, and the total length of the root hair. Compared to the control, the inoculated root hairs exhibited nuclei that were on average closer to the tip of the root hair for the fourth and fifth days of observation. The ratio of the nucleus-to-tip distance over the total length of the root hair was also significantly lower in the inoculated group than in the control. Additionally, the average distance between the root hair nuclei and the tip of the root hairs on those days was close to the reported nucleus-to-tip distance that occurs during stages of tip growth in root hairs. This suggests that the root hairs may have been in a state of tip growth at this stage after inoculation, perhaps in anticipation of tip growth for root hair curling, although specific root hairs were not tracked. More investigation is needed in order to understand the nuclear dynamics in root hairs, especially with regard to the activity of specific root hairs over time and root hairs of similar lengths. These experiments will be the basis for investigation into the molecular dynamics and potential connections between early stages of nodulation and nuclear movement.

INTRODUCTION

Symbiotic relationships

Symbiotic relationships are tightly regulated, co-evolved systems between organisms. These close-knit interactions have been crucial in the generation of biological diversity over time (Moran, 2006). Mutualistic symbioses are ecologically significant, and a mutualistic interaction increases the overall fitness of each symbiotic partner. Microbes that associate with eukaryotes tend to act as metabolic partners that provide the eukaryote with access to limiting nutrients such as nitrogen. Terrestrial ecosystems rely on mutualistic partnerships between land plants and their fungal and bacterial symbionts (Moran, 2006). Nitrogen-fixing bacteria are particularly important for the conversion of atmospheric nitrogen into forms usable by plants, and after decomposition of this plant matter, nitrogen will return to the ecosystem (reviewed in Troyo-Dieguez et al., 2010).

Rhizobia are members of the phylogenetically diverse group of soil bacteria that engage in symbiotic partnerships with leguminous plants (family Fabaceae). This symbiosis is one of the most important ecological interactions to both humans and ecosystems (Ackay and Roughgarden, 2007; Fournier et al. 2008; Fournier et al. 2015). For many ecosystems, the partnership between legumes and rhizobia provides the most significant input of nitrogen to the system (Ackay and Roughgarden, 2007). Once rhizobia present within soil begin to coordinate with a host legume, an extensive amount of signal exchange occurs (Ackay and Roughgarden, 2007). This communication, when successful, eventually gives rise to a nitrogen-fixing nodule within the root. Globally, nodulated legumes are useful for human food, forage, and other purposes such as pharmaceuticals (Werner and Newton, 2005). Agriculturally, the economic and environmental costs of relying on nitrogen fertilizers are an increasing concern, and biological nitrogen fixation is a facet of sustainable and environmentally friendly food production (reviewed in Troyo-Dieguez et al., 2010). Increasing our understanding of the complexities of symbiotic nodulation mechanisms could be useful in the engineering of legumes for agricultural and ecological benefit.

Mechanism of infection

The rhizobial symbiont for the model legume *Medicago truncatula* is *Sinorhizobium meliloti*. For symbiosis to occur in legumes, bacteria must first colonize their host through epidermal root hairs (Gage, 2002; Fournier et al. 2008). Furthermore, host and microbe must be able to recognize and interface with one another for symbiosis to progress successfully. This is achieved through a dialogue of plant- and bacteria-derived compounds. Legumes secrete phenolic compounds known as strigolactones into the soil that are perceived by nearby rhizobia. Upon strigolactone perception, rhizobia secrete lipo-chitooligosaccharides called Nodulation (Nod) factors (reviewed in Oldroyd, 2013). These, in turn, are perceived by the plant, which induces several cellular and tissue-wide changes to prepare for accommodation of the symbiotic microbe (Van Bruaene et al., 2004; reviewed in Oldroyd 2013).

Molecular and cellular changes

Various cellular responses occur in the host's root hairs prior to infection: calcium oscillations, tip growth reorientation (root hair curling), and divisions of inner cortical cells preceding nodule primordium formation (Peiter et al., 2007; Oldroyd and Downie 2008; Timmers, 2008; Sieberer et al. 2012). Nod factors induce plasma membrane depolarization and calcium spiking (cytosolic calcium oscillations) (Oldroyd 2013). During Nod factor-induced calcium spiking, the nuclear envelope and nuclear-associated endoplasmic reticulum are likely to be the internal stores for calcium-induced spiking (Peiter et al., 2007; Oldroyd and Downie, 2008).

As the root hair receives these signals, it undergoes tip growth in order to grow and curl around

adjacent rhizobia, enclosing them in the space outside of the plasma membrane (Genre et al., 2005; Werner and Newton, 2005; Murray et al., 2011). Sites of infection are characterized by concentration of cell protoplasm and the movement of the cell nucleus to these regions (Fahraeus, 1957; Oldroyd and Downie, 2008, Fournier et al., 2008). The cell wall of the root hair is subsequently degraded and the plasma membrane of the cell invaginates (Gage, 2004). These enclosed spaces are called "infection chambers," and can also be created when a rhizobium is trapped in the space between two touching root hairs. (Gage, 2004; Fournier et al. 2008; 2015).

From this infection chamber, the plasma membrane continues to invaginate and begins to form a host-driven structure known as an infection thread (IT) (reviewed in Oldroyd, 2013). As the IT initiates, the growth of the root hair tips halts, and the nucleus disengages from the site of rhizobial penetration and is repositioned ahead of the advancing IT tip, moving down the body of the root hair cell (Timmers 2008; Morieri et al., 2013; Perrine-Walker et al., 2014; Kitaeva et al., 2016). The plasma membrane invagination expands, tracking with the nucleus down the root hair body, forming a tubular structure known as the infection thread (Gage, 2004). Rhizobia proliferate in the infection chamber, and then enter the IT and continue to divide (Fournier et al., 2008, 2015). Infection begins through this apoplastic invasion of the root hair, extending from the site of infection toward the basal part of the root hair and eventually reaching the cortex and inner cortex of the root (Timmers et al., 1999; Genre et al., 2005; reviewed in Oldroyd, 2013).

Despite this knowledge of the link between nuclear dynamics and infection during infection thread initiation and growth, the details of nuclear movement and positioning in before IT initiation are not well characterized. Anecdotal evidence places the root hair nucleus at the site of cell wall remodeling (Timmers et al., 1999), but not much information has been collected regarding the nucleus' role in initial infection contact at the onset of root hair remodeling. Nuclear movement has been shown to be linked to arbuscular mycorrhizal infections, and in general movement and positioning of the nucleus appears to be tied to major developmental processes and cell responses (Fournier et al., 2008; Oldroyd and Downie, 2008; Parniske, 2008; Murrary et al., 2011; Oldroyd, 2013).

OBJECTIVES

Many papers have focused on the signaling interaction between host and microbe, remodeling during infection thread formation, and bacterial multiplication through the infection thread (Turgeon and Bauer, 1985; Catoira et al., 2001; Fournier et al., 2008, 2015). However, the cellular dynamics that precede root hair curling and subsequent infection have not been well documented.

To my knowledge, only one study has specifically focused on subcellular dynamics after the crosstalk between rhizobia and plant has begun, but before the initiation of symbiosis. Sieberer and Emons (2000) documented that, in tip-growing *Medicago truncatula* root hairs, the nucleus maintains a distance from the tip of 30±5 μm on average, and that in growth-terminating root hairs (the subpopulation that they observed deforming in response to Nod factors), this tip distance increases. They observed that, upon application of Nod factors, the growth-terminated cells restarted tip growth, with the nucleus returning to its previous position of 30±5 μm from the tip of the new outgrowth. However, this study did not specifically focus on documenting the movement of the nucleus, nor did they use modern imaging techniques. Furthermore, rather than utilizing the biologically representative system of applying rhizobia to roots, they relied on Nod factors to act as a proxy for the symbiont. I hope to add to this field by generating a set of data focusing specifically on the nucleus during the early stages of development, using the actual symbiont as my stimulus.

The main challenge with documenting these early stages of rhizobial infection is the frequency of root hair responses to Nod factors versus the number of root hairs that have infection events. While pre-infection responses to NFs are observed in the majority of Root hairs, infection threads will only be formed in a subset of these (Journet et al. 2001; Wais et al., 2002; Boisson-Dernier et al. 2005). Fournier

et al. (2008) addressed this issue somewhat by using a super-nodulating mutant *sunn* (super numeric nodules), which have approximately 10 times as many infection events as WT. They observed root hair curling 4 to 5 days after rhizobial inoculation in both WT and the sunn mutant. However, this method does not include the possibility of using modern fluorescence microscopy to track the nucleus. Therefore, I decided to tweak the methods of previous successful studies to be both more applicable to wild type situation and more adaptable to stable nuclear marker lines so that this methodology may later be used for the study of nuclear movement defect phenotypes.

While it has been observed that the nucleus seems to be linked to the formation of the IT, most research has been focused on the nucleus leading the extending infection thread (reviewed in Oldoryd, 2013; Fournier et al., 2008, 2015). However, the movement and position of the nucleus may further be important at earlier stages of infection (Sieberer et al., 2009; Fournier et al., 2015). As discussed above, studies have observed the dynamics between the application of purified Nod factors and root hair curling, the effects on root hair ER, and nearby cortical cell divisions, but they have not described the details of how the nucleus is involved in infection (Bladergroen and Spaink, 1998; Catoira et al., 2001; Timmers, 2008; Charpentier et al., 2016). While the nucleus has anecdotally been observed to move toward the tip of the root hair that is curling in response to rhizobial Nod factors (Timmers et al., 1999), studies have not specifically looked at the position, movement, or shape during the infection process.

For this thesis, I aimed to document the initial process of infection thread formation between the model organism legume *Medicago truncatula* (Figure 1.1) and its rhizobial symbiont, *Sinorhizobium meliloti* (Figure 1.2). To do this, I adapted confocal microscopy and a live on-plate imaging technique (Figure 2.1) that has been used to track other organelles previously during the preliminary stages of symbiosis initiation (Genre et al., 2005; Fournier et al. 2008; 2015). I conducted time course imaging experiments to identify optimal imaging conditions and timing of post-inoculation observations, monitored infected *Medicago truncatula* seedlings over various time periods, and tracked root hairs with putative infection morphologies to map out the temporal dynamics of early infection prior to root hair curling.

To track nuclei during infection, I used a stably transformed *Medicago truncatula* line with the fluorescent nuclear marker NLS-YC3.6 (Figure 3.1-3.2). To monitor rhizobia during infection, I used a dsRed-labeled *Sinorhizobium meliloti* 2011 strain. Used together, these allowed me to monitor both the host plant and the rhizobia using confocal microscopy. My goal was to detail how nuclear movement is connected to the observed changes in root hair morphology and rhizobial positioning prior to the formation of the infection thread in the root hair. I chose to focus on the period of time prior to full curling of root hairs and the formation of infection threads. I adapted methods from previous studies to focus on

Figure 1.1. *M. truncatula* in pot, **(a)** mature, **(b)** young.

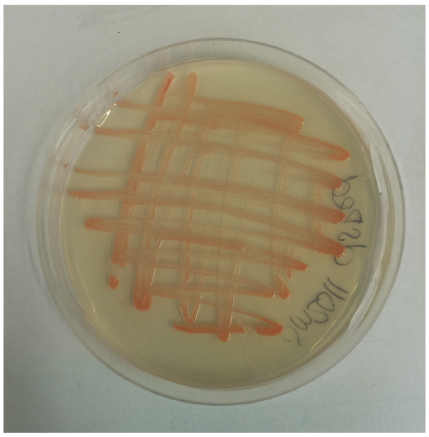

Figure 1.2. *Sinorhizobium meliloti* on TY agar plate.

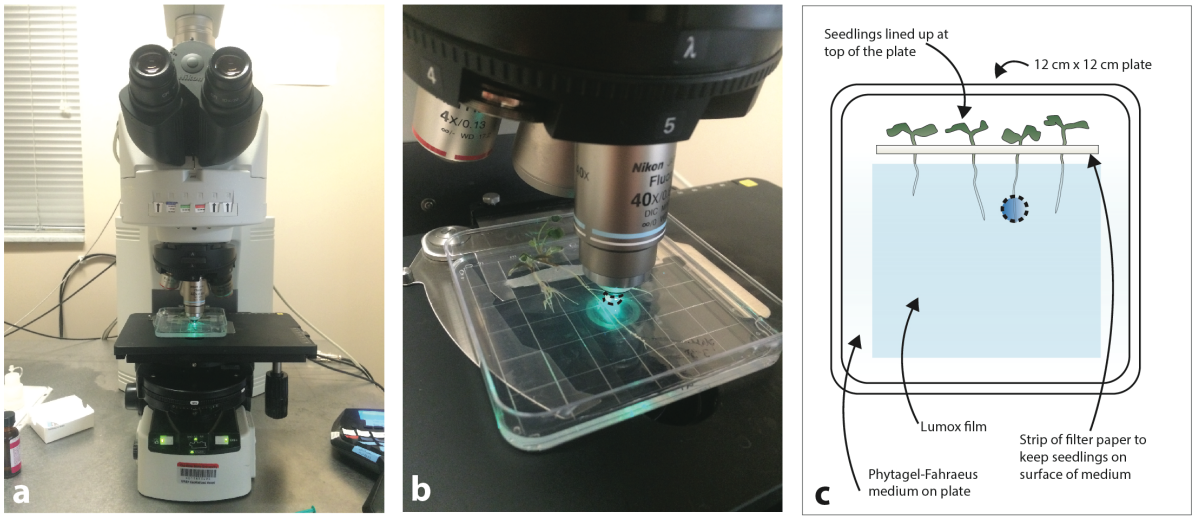

Figure 2.1. (a, b) Confocal microscope, with plate of seedlings under the 40X water immersion objective. The black dashed line in **(b, c)** shows the bead of water that makes contact with both the water immersion objective and the Lumox film. The adhesion between the water and both surfaces allows the droplet to move as the plate is shifted beneath the objective. **(c)** The seedlings are arranged in a row on the solid medium. Because they do not stick well to the surface of the medium, a thin strip of filter paper was used to help keep them in position.

the 1 to 5 day period following inoculation to see if changes in nuclear movement and position would be distinguishable prior to curling (Fournier et al., 2008). It is not well known how many root hairs may be responding to the presence of Nod factors, nor how many of these root hairs will actually begin to develop nodules. During analysis, any root hair curling or displaying the morphology of a root hair interacting with rhizobia may be measured. This will capture a more comprehensive overview of how root hairs subjected to the presence of rhizobia respond, and it will not be narrowly focused only on the root hairs fated for nodulation (i.e., already exhibiting curling). Hopefully understanding the wide range of root hair responses

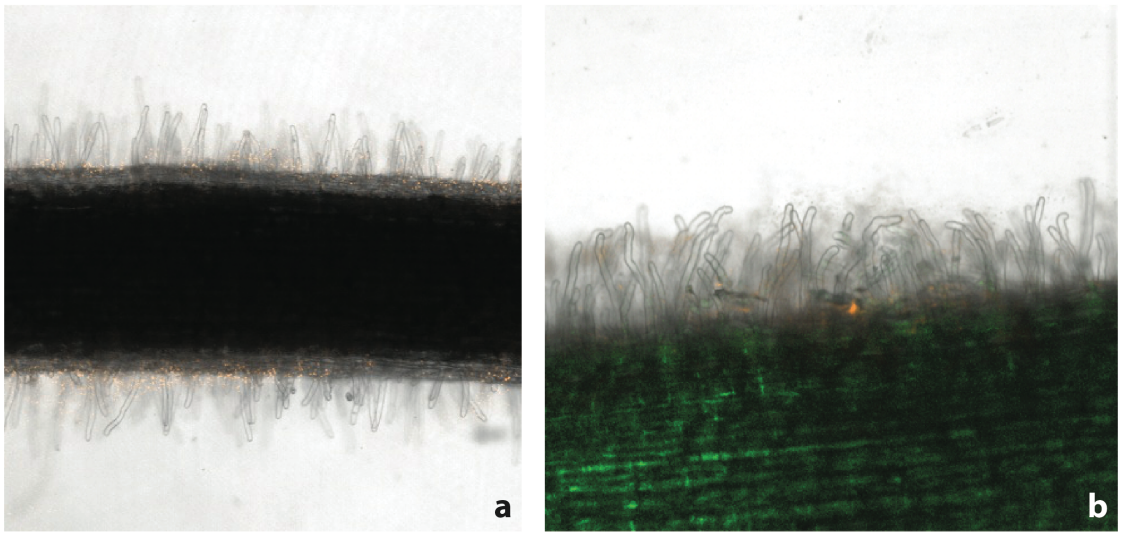

Figure 3.1. Root morphologies using the 4x objective. Here, the density and distribution of root hairs can be seen projecting from the root. **(a)** *M. truncatula* R108 wild type root with *S. meliloti* 2011 dsRed, **(b)** *M. truncatula* R108 wild type with the YC3.6 nuclear marker root with *S. meliloti* 2011 dsRed.

will allow for later pinpointing of the precise root hair activity that seems to lead to successful complete infection and nodulation. The primary objective of my project was to establish quality baseline information, both qualitative and quantitative, about the movement of root hair nuclei during the initiation of nodulation. I wanted to document the process of nuclear movement during the very initial stages of symbiosis and the concomitant morphological changes in infected root hairs.

RESULTS

Summary

First, I determined the optimal methods and imaging conditions for the earliest stages of infection thread development. This investigation was mainly performed by reviewing previous literature on this subject (beginning with Fahraeus' 1957 study on clover) and attempting to replicate reported methods with a stable *Medicago truncatula* nuclear marker line (YC3.6; obtained from Myriam Charpentier, John Innes Center, Norwich, UK, see below) and *Sinorhizobium meliloti* dsRed strain (obtained from Myriam Charpentier, John Innes Center, Norwich, UK, see below). I experimented with blending various techniques of plating and maintaining seedlings, imaging conditions, and timing. I have compiled and adapted various imaging and infection techniques from multiple previous papers to determine optimal conditions for healthy root hair growth, rhizobia survivorship, and overall image clarity.

After plants and rhizobia could be grown consistently, I verified their fluorescent signatures and established optimal conditions for confocal microscopy on the Nikon Eclipse 90i microscope. I tested various time course patterns and imaging types (single image, z-stack) to determine the ideal method for capturing root hairs of the YC3.6 line.

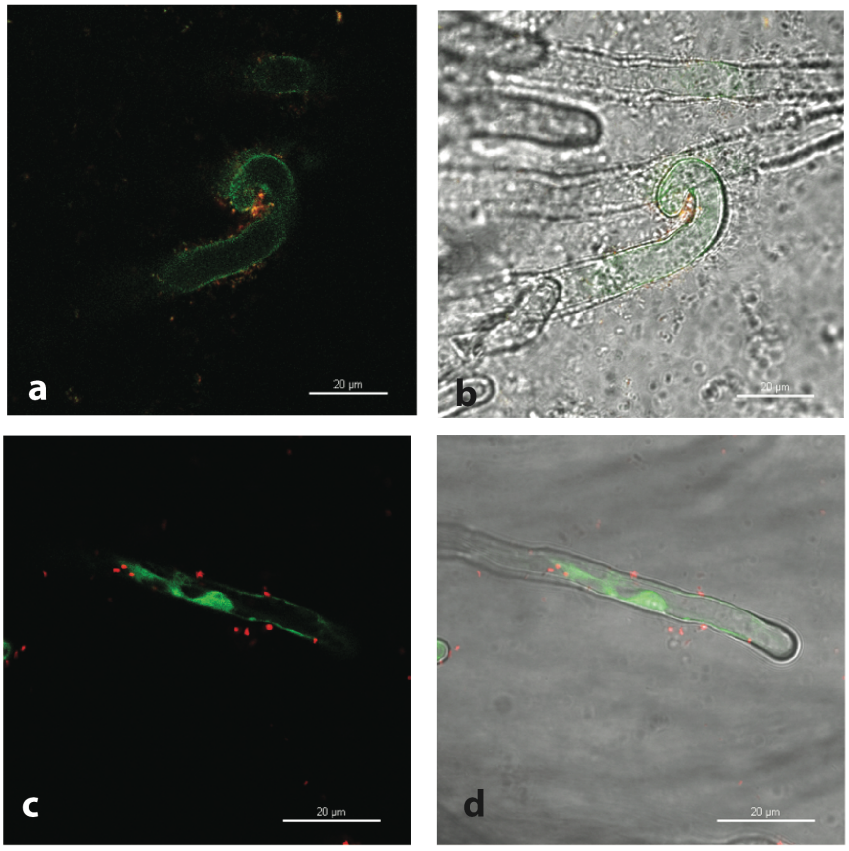

Figure 3.2. (a, b) Endogenous fluorescence in *M. truncatula* root hairs. **(c, d)** Visual validation of the nuclear marker using the confocal microscope. Scale bar, 20 μm.

I measured several metrics for the root hair, including distance from the middle of the nucleus to the tip of the root hair, as well as total root hair length, to generate quantitative information about nuclear positioning during this period. To analyze my data, I explored software and plugin options within several visualization and statistical programs. I tested the following programs to find different tools for better analysis of this particular system: NIS-Elements AR, ImageJ/FIJI (Schindelin et al., 2012), Icy (de Chaumont et al., 2012), MeshLab (Cignoni et al., 2008), and Python scripting (see Table 1 in methods for version numbers). Icy (Quantitative Image Analysis Unit at Institute Pasteur) is popular among biotechnology and biomedical researchers. It is well-documented, its plugins are also described online, has ImageJ integrated into its interface, and can connect to Matlab. For these reasons, for observations involving complex 3D spaces and dynamics, I used Icy for visualizations during data collection.

Part 1: Methodology refinement

Growth conditions

Prior to observing nuclear movement and positioning in a quantitative manner, I wanted to review the various available materials and methods for infections to see what would work well for the R108 ecotype of *M. truncatula*. Although there are more recent papers on the topic of infection imaging, many of them refer to Gosta Fahraeus' 1957 paper (Fahraeus et al., 1957; Catoira et al., 2000; Haynes et al., 2004; Gage, 2002; Moirieri et al., 2013; Fournier et al., 2015). This appears to be the first instance of a technique in which continuous and repeated observations of the growth and infection of root hairs can be performed, although the focus was on clover (Trifolium repens) (Fahraeus, 1957). Growth medium is layered between a coverslip and microscope slide, and the seedling is grown in this media-filled space between the two pieces of glass. Seedlings are kept sterile in vials containing a solution inoculated with a suspension of the clover's symbiont, Rhizobium trifolii (Fahraeus, 1957). This method was challenging to replicate, and in most cases root growth was poor (modified Fahraeus media (modFP), see methods for composition) (Figure 4.1a). I followed the described technique using *M. truncatula* and *S. meliloti*. When left long enough, the *M. truncatula* plants would grow roots horizontally to the edge of the medium, and then they would grow downward (Figure 4.1a) into the inoculated liquid media and eventually develop nodules. However, by this point the plants had grown away from the glass containment need for imaging (Figure 4.1a). After many attempts and only one successful slide, this technique was abandoned despite its potential utility: it would have allowed for the use of higher magnification objectives since the slide could be used with high magnification oil immersion objectives.

I turned to the on-plate live imaging technique, which allows the same repeated and continuous observation as the Fahraeus slides (Genre et al., 2005; Fournier et al. 2008). Fournier et al. (2008) started their seedlings on agar-Fahraeus medium, so I used this initially. After I observed stunted seedling growth on this medium, I learned that Whatman filter paper (Fisher Scientific, 09-924-349) can be used to regulate nutrient uptake and prevent agar-sensitive Medicago from contacting the media directly (Kuster et al., 2006; Myriam Charpentier, personal communication). I therefore attempted to grow seedlings with this filter paper layered between the seedling roots and the media. Although the filter paper method did provide the added benefit of preventing the seedling roots from penetrating the media, it required that the seedlings be moved to another plate for imaging because during microscopy young root hairs were too similar in appearance to the filter paper fibers. Transferring the seedlings to a plate without filter paper also increases the risk of contamination of the plates. Additionally, mechanical stress may influence the cytosolic calcium spiking in root hairs (Swanson and Gilroy, 2013).

To get around these drawbacks, I utilized an alternative polymerization method for my solid media. Fournier et al. (2008) report the use of an agar substitute called Phytagel (Sigma-Aldrich, P8169). In their protocol, seedlings are grown on agar-Fahraeus medium (Boisson-Dernier et al., 2001) for a week before being transferred to Phytagel plates (Fournier et al., 2008, 2015). However, I decided to use only

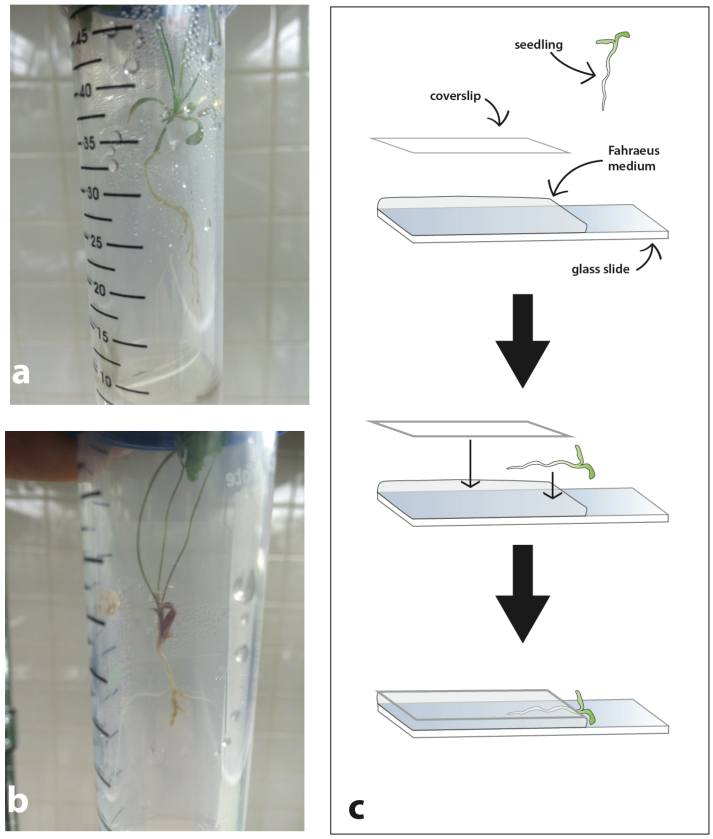

Figure 4.1. *Medicago truncatula* grown using the Fahraeus slide method. **(a**) Photograph showing the seedling partially escaping the layer of medium between the glass slide and coverslip. **(b)** Photograph showing the stunted root growth of *M. truncatula* seedling on a Fahraeus slide. **(c)** Diagram of Fahraeus slide assembly.

Phytagel-Fahraeus medium since the seedlings did not grow well on agar. The Fournier et al. (2008) Phytagel medium was a modified Fahraeus (modFP) recipe supplemented with 2-aminoethoxyvinylglycine (AVG) and 0.5% [w/v] Phytagel (Fournier et al., 2008, see methods for details). AVG is included because it may inhibit the production of ethylene, which has been shown to limit the production of nodules (reviewed in Guinel and Geil, 2002). Additionally, although AVG appears to allow more nodules to form, the nodules still arise in the normally responsive roots of the plant (Peters and Crist-Estes, 1989). A previous study experimented with the various concentrations of AVG to stimulate nodulation (Peters and Crist-Estes, 1989), but a restricted concentration of AVG must be used while plating this construct because increased concentration of AVG seem to greatly reduce the fluorescence of the YC3.6 reporter (data not shown; fluorescence levels were very low during imaging and at the normal gain used the signals were visually undetectable). Using Phytagel-Fahraeus medium with AVG, plants were grown vertically on their plates (Figure 5.1a). Seedlings often did not stick well on the surface of the medium (Figure 5.1b), so a thin strip of Whatman filter paper was used to keep the seedlings in position on their plate (Figure 5.2) (see methods).

To stimulate lateral root growth, I severed *Medicago truncatula* seedlings just above the root tip (Fournier et al., 2008). Fournier et al. (2008) perform this modification in order create more available root hairs for infection. However, this increases the overall length of an experiment as it takes about five additional days for the new lateral roots to initiate. Initial observations suggest that nodules will occur on both the main root and the lateral roots if given enough time and space; anecdotally, inducing branching by truncating the roots does provide more root system surface area for rhizobial infection. This also provided more individual root hairs that could be candidates for observation and infection. However, the additional time necessary outweighed the benefit in terms of infection events, and I did not continue with this method.

One of the most useful features of these studies was the use of Lumox film (Sarstedt, Inc., cat. no. 94.6077.317), which is gas-permeable, transparent plastic film that has the same refractive index as water and permits the use of water immersion objectives directly on the plant roots on their plate (Genre et al., 2005; Fournier et al., 2008, 2015; Figure 2.1). This has been shown to be effective in imaging of root symbioses, especially after the preliminary experiments in image capture methods (Genre et al., 2005). Fournier et al. (2008, 2015) report that they left their gas- permeable film on the plates between

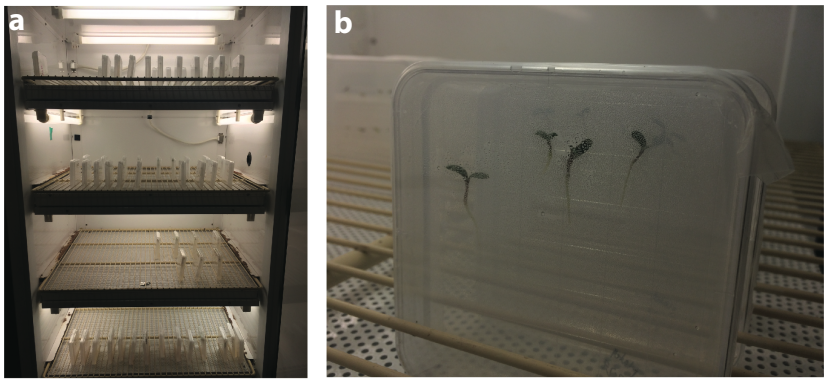

Figure 5.1. (a) The growth chamber has racks that keep the plates upright so that the seedlings grow vertically. **(b)** The seedlings were prone to falling off the of Phytagel medium, and they did not grow as well if they ended up displaced on the lid of the plate or with their roots not contacting the medium.

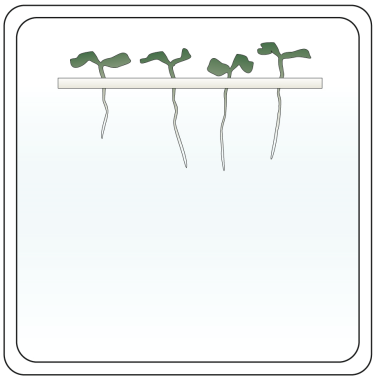

Figure 5.2. A thin strip of filter paper was enough to keep the seedlings in position. This plate set up was used for all experiments where quantitative data was collected.

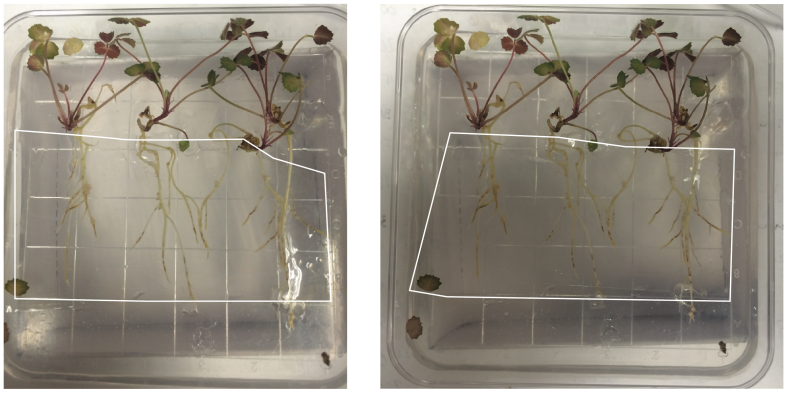

Figure 6.1. YC3.6 *M. truncatula* seedlings with *S. meliloti*, roots covered in Lumox plastic film at time of inoculation. Image taken ~ 20 days after the addition of the film and inoculation. The white line was added to the image to outline the edge of the film, since it is difficult to see.

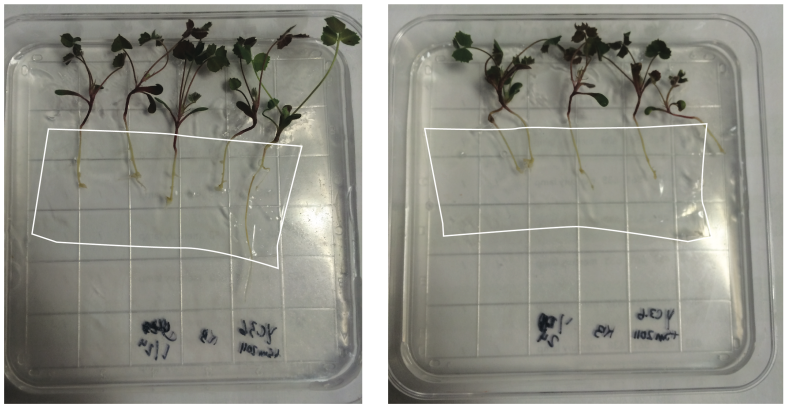

Figure 6.2. YC3.6 *M. truncatula* seedlings with *S. meliloti*, roots covered in Lumox plastic film a week after inoculation. Image taken ~ 10 days following the addition of the Lumox film The white line was added to the image to outline the edge of the film, since it is difficult to see.

imaging sessions, but my seedlings seemed additionally stressed and grew poorly when they were covered with Lumox film at the time of inoculation (Figure 6.1). If seedlings were covered a week after inoculation, they were able to produce nodules but the roots did not appear healthy (Figure 6.2). Therefore I only kept the film on the seedlings while imaging (Figure 2.1a-b).

For my experiments, I set up plates of seedlings for “inoculated” and “uninoculated” treatments. The seedlings to be imaged on a given day were germinated together and then separated. The inoculation group was sprayed with rhizobia suspended in water (see methods for details). The uninoculated plants were treated in the same manner as the inoculated plants but sprayed using only water so that they two treatment groups received the same amount of initial moisture.

Imaging conditions

With the plants able to grow and survive reliably (while remaining

observable with confocal microscopy), I started exploring the plant root hairs and their growth tendencies. The benefit of confocal microscopy is that it allows the observation of a single section in the volumetric axis. This allows for visualization of subcellular structures without interference from fluorescence above or below it. However, upon preliminary imaging of Medicago root hairs, it became evident that single images would lack sufficient information (Figure 7.1), with the exception of observing a single nucleus at a high optical zoom (Figure 7.2). This is largely because root hairs do not grow in two dimensions, but in three. By observing a single confocal section, I could only see a small amount of a given root hair, prohibiting measurements such as distance from root hair nucleus to tip or full root hair length (Figure 8.1). Therefore, generating projections over multiple sections in the volumetric, or z, axis would allow me to observe and measure root hairs in their entirety. These projections are known as z-stacks, and they were determined to be the ideal image capture method as they provide an image of the full root hair in focus (Figure 8.2).

Z-stacks were examined in both open-source programs like ImageJ and Icy as well as proprietary software NIS-Elements AR (v. 3.2) (Figures 9.1-9.3). All three of these programs provide built-in tools for measurements and quantifications. In the case of ImageJ, a plethora of plug-ins and macros for other types of measurement, visualization, and examination are available, and they can be incorporated individually or downloaded as FIJI (a version of ImageJ with plugins included) (Schindelin et al., 2012). Because of their 3-dimensional shapes and growth patterns (Figure 7.1), plant root hairs are a cell type that could benefit from modern digital 3D models and animations. Confocal imaging with fluorescent markers is an ideal image capture technique for 3D projections and modeling through Z-dimension focus stack imaging. I chose to use ImageJ for measurements because it is relatively easy to use, but I also explored alternative methods for image analysis. Icy (Quantitative Image Analysis Unit at Institute Pasteur) is popular among biotechnology and biomedical researchers. Icy is fairly well-documented (although not as much as ImageJ) and its plugins are also described online. It has ImageJ integrated into its interface and can connect to Matlab as well. For observations involving complex 3D spaces and dynamics, Icy has a much more polished user interface (Figure 9.3c) compared to ImageJ, and its ability

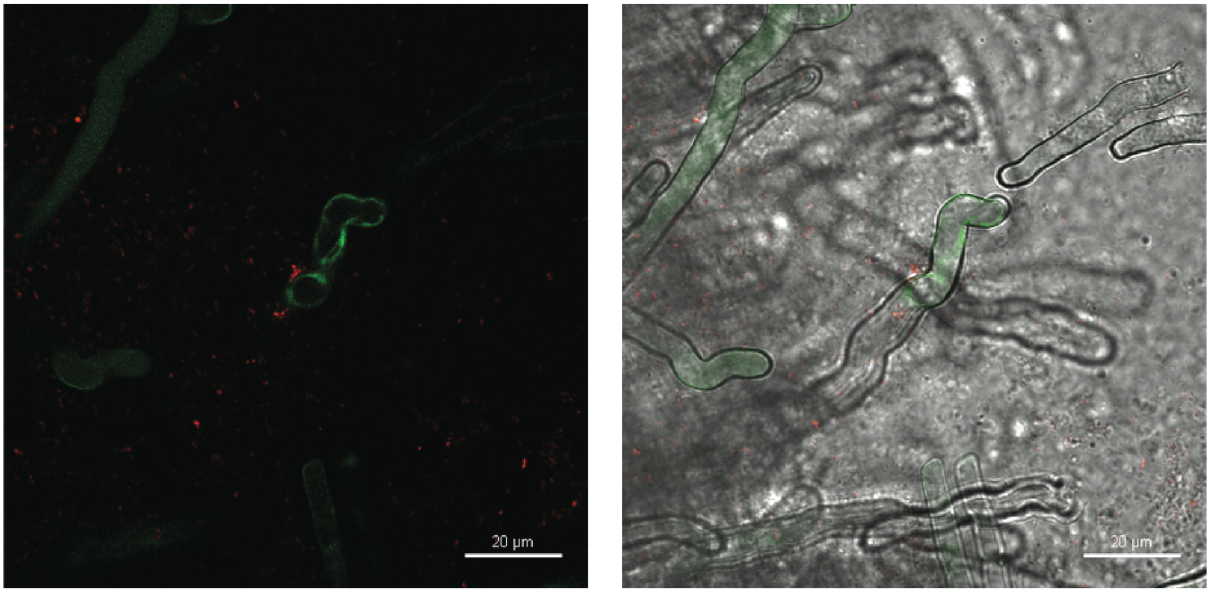

Figure 7.1. Example of single section of root hairs. Fluorescence is only visible in the current optical section. Without the rest of the root hair, it is not possible to assess the total fluorescence profile, size of the root hair, or the position of the nucleus. GFP signal is the YC3.6 nuclear marker in *M. truncatula*, and red is the dsRed *S. meliloti. Scale bar, 20 µm.*

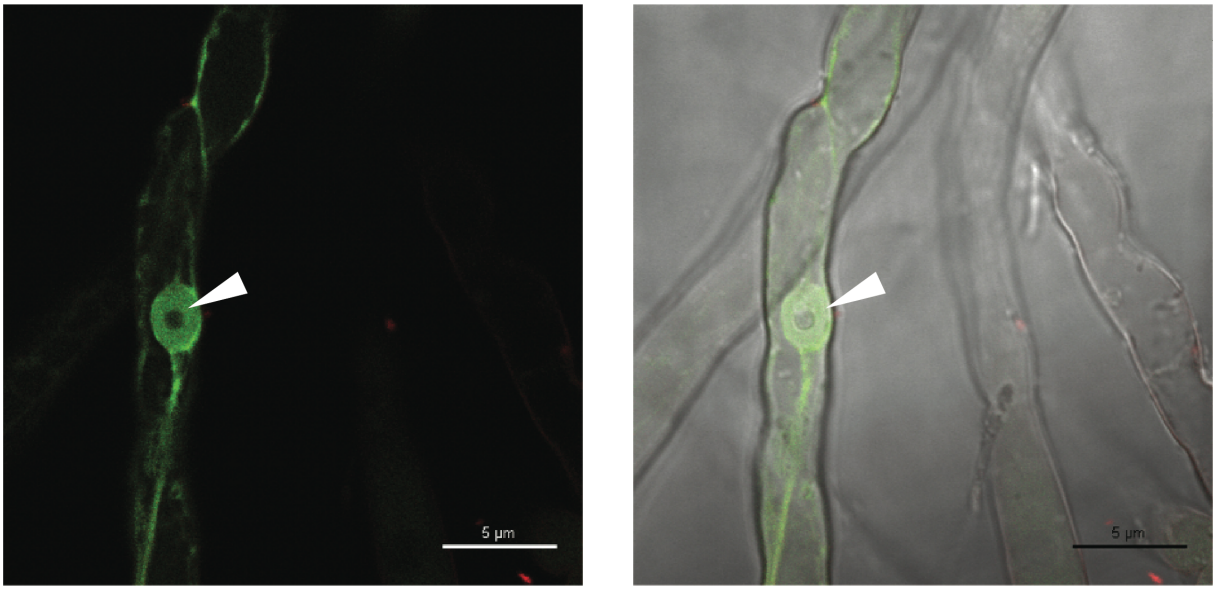

Figure 7.2. Examples of a nucleus at a high optical zoom. Here, the nucleus is well marked by the calcium nuclear marker and the nucleolus (white arrow) can be seen. GFP signal is the YC3.6 nuclear marker in *M. truncatula*, and red is the dsRed *S. meliloti.* Scale bar, 5 *µ*m.

to manipulate channels is much more advanced than ImageJ. Many of ImageJ's functions are buried in their dropdown menus and lists; Icy has an organized GUI with a convenient side panel to change channels colors, view ROI measurements, and more (Figure 9.3c). A drawback of Icy is the lack of information online describing its functions; ImageJ is much more popular and has more online resources. Table 1 (see methods) shows a breakdown of some of the advantages and disadvantages of the software explored here. Ultimately, images were analyzed using ImageJ 3D projections, maximum intensity projections, and sections from the image z stacks (Figure 9.2; Figure 11.1). For quantifications, ImageJ measurement tools were used, and data was analyzed in OpenOffice Calc (see Part 2: Analysis for details).

3D models and projections were generated using ImageJ (and plugins), Icy, and Python scripting with MeshLab.. ImageJ imports metadata regarding the calibrated measurements of the pixels, so all of its outputs are in the desired units. Icy was used to generate a maximum intensity projection during measuring; having a compilation of the stack while analyzing images helps give a frame of reference for following the path of root hairs through the z dimension. When the z-stacks have many overlapping root hairs, 3D projections in Icy or ImageJ can be used to see the position of the root hairs in space and make it easier to see where they are in the stack.

I devised a method for composing interactive 3D models of this system. 3D projections from ImageJ and Icy are built by processing image data in a stack and calculating the viewing angle. However, the output is still a 2D rendered image because this type of information does not correspond to volumetric data. 3D projections also demand lots of processing power if the viewer wants to turn or manipulate the view angle. This is because the projection must be rendered over and over again with any adjustments that are made. With the help of a collaborator (Taylor Driggs, personal correspondence), I wrote a Python script for processing the images of a stack and then converting the 2D fluorescence information into a 3D point cloud, which can be viewed in the open source software, MeshLab (Figure 10.1-10.2).

Figure 8.1. (a) Example of single sections of root hairs. Fluorescence is only visible in the current optical section. Without the rest of the root hair, it is not possible to assess the total fluorescence profile, size of the root hair, or the position of the nucleus. The stack was exported to individual images using ImageJ, which typically imports channels in grey scale (as shown here) unless a color is specified. The white in this sequence is the GFP signal. Scale bar, 10 μm (in first image of sequence).

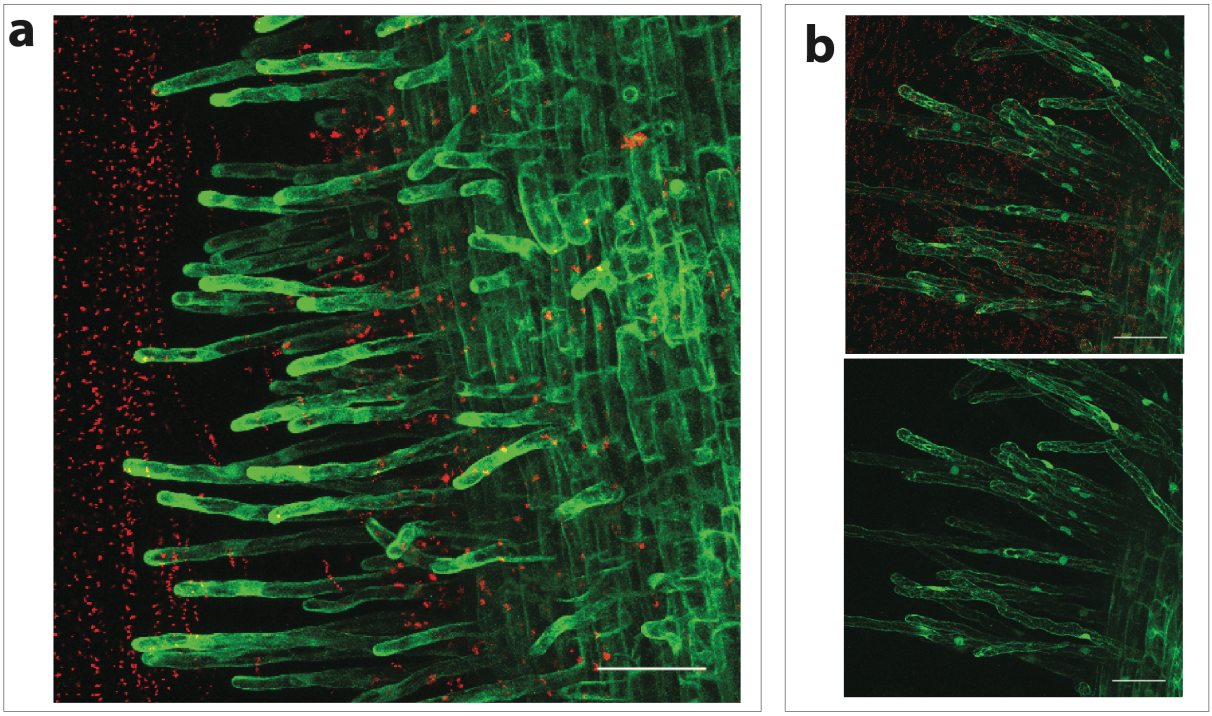

Figure 8.2. (a, b) Examples of maximum intensity projections from Icy. GFP of the YC3.6 marker in *M. truncatula* is green; dsRed marker for *S. meliloti* is red. Scale bar, 50 μm.

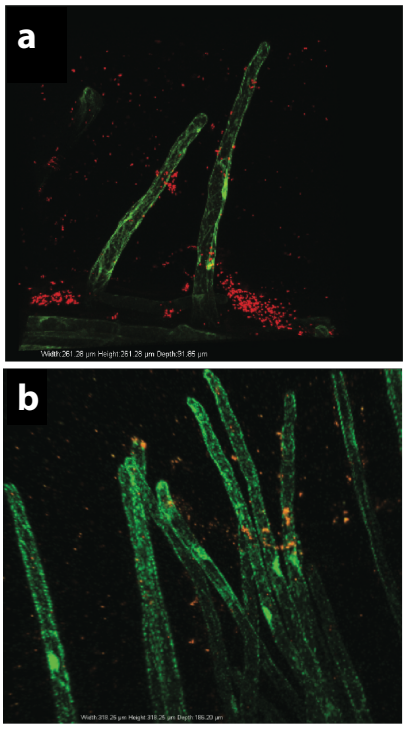

Figure 9.1. (a, b) NIS Element AR 3D projection of C3.6 Medicago truncatula root hairs (from the inoculated group). NIS Elements AR uses maximum intensity to show the fluorescence data volumetrically. The projections are relatively easy to view, but they can only be opened with NIS Elements AR. Screenshots and videos can be captured, but the software is somewhat slow. Scale bars not shown -- dimensions are given on the 3D projections for width, height, and depth.

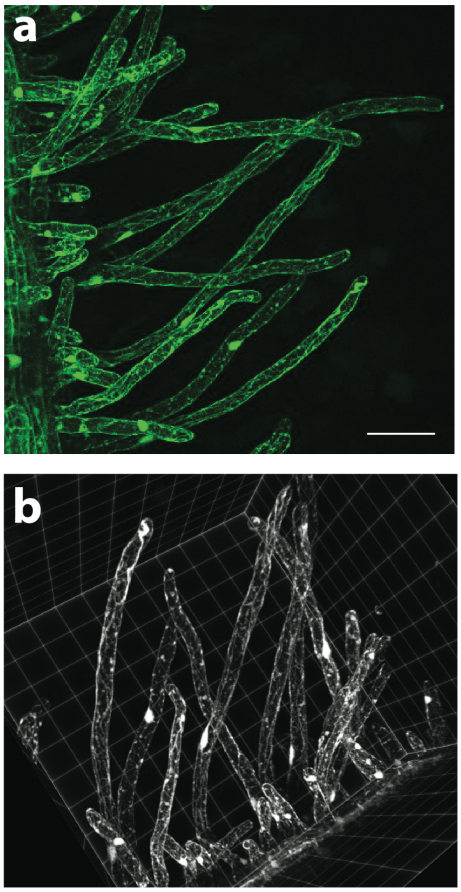

Figure 9.2. (a) ImageJ maximum intensity projection of C3.6 Medicago truncatula root hairs (from the inoculated group; rhizobia not shown). **(b)** This ImageJ 3D projection is of the same z stack as **(a)**. ImageJ 3D projections, especially those made using the ClearVolume plugin, have the advantage of being the easiest to rotate and view. The 3D model and maximum intensity projections of z stacks, like **(a and b)** were not directly measured, but they were useful visual aids for determining how the root hairs were arranged in space.

Part 2: Analysis

Seeds that were to be imaged on the same day were scarified, sterilized, and germinated on the same day so as to be synchronized (see methods). Once germinated, seedlings were transferred to plates with Phytagel-Fahraeus medium (see methods) for one week prior to inoculation. Plates were subsequently divided into two groups (Experimental Design 1). Half were inoculated with rhizobial cultures (as described in methods), and the other half were sprayed with an equal volume of water. Then, seedlings were stored in the incubator for 24 hours before being imaged for Day 1 (Experimental Design 1). Seedlings were covered with Lumox film and imaged using z stacks. I took the z stacks by selecting a section that was slightly above the top most point of fluorescence in a given region of root hairs, and then selected another section that was slightly below the bottom most point of fluorescence. The purpose of this is to capture the definitive edge of the root hair to make sure the entire cell is in focus.

Suitable root hairs were selected based on overall availability and their zone. Root hairs grow in the region of maturation. In order to methodically identify the region of maximal root hair growth on a given day, the root tip was first located. I then navigated up the root until root hairs were visible. Areas of roots hairs were skipped if they were too tangled to be reliably measured or if the root hairs were too long to fit within the frame of the image. The dimensions with the 40X objective were 318.5 x 318.5 µm, so root hairs that were too large to fit within

that area were not measured. For Day 2, I approached using the same protocol on the plates imaged the day before. This was repeated for Day 3, 4, and 5 (Experimental Design 1). This method used root hairs of roughly the same age and developmental stage because the same zone on the root hair is imaged every time (not the same root hairs previously imaged, which would be older at the next time of imaging). Each day, 7-10 images were taken per treatment, with multiple root hairs in a given image, to try to capture enough root hairs with visible nuclei. It was difficult to see everything that is present until the z stack were reconstructed and viewed later. The 40x objective generates an image that is 318.5 x 318.5 µm, so the entire length of a root hair had to fit within those dimensions in order to be used in data

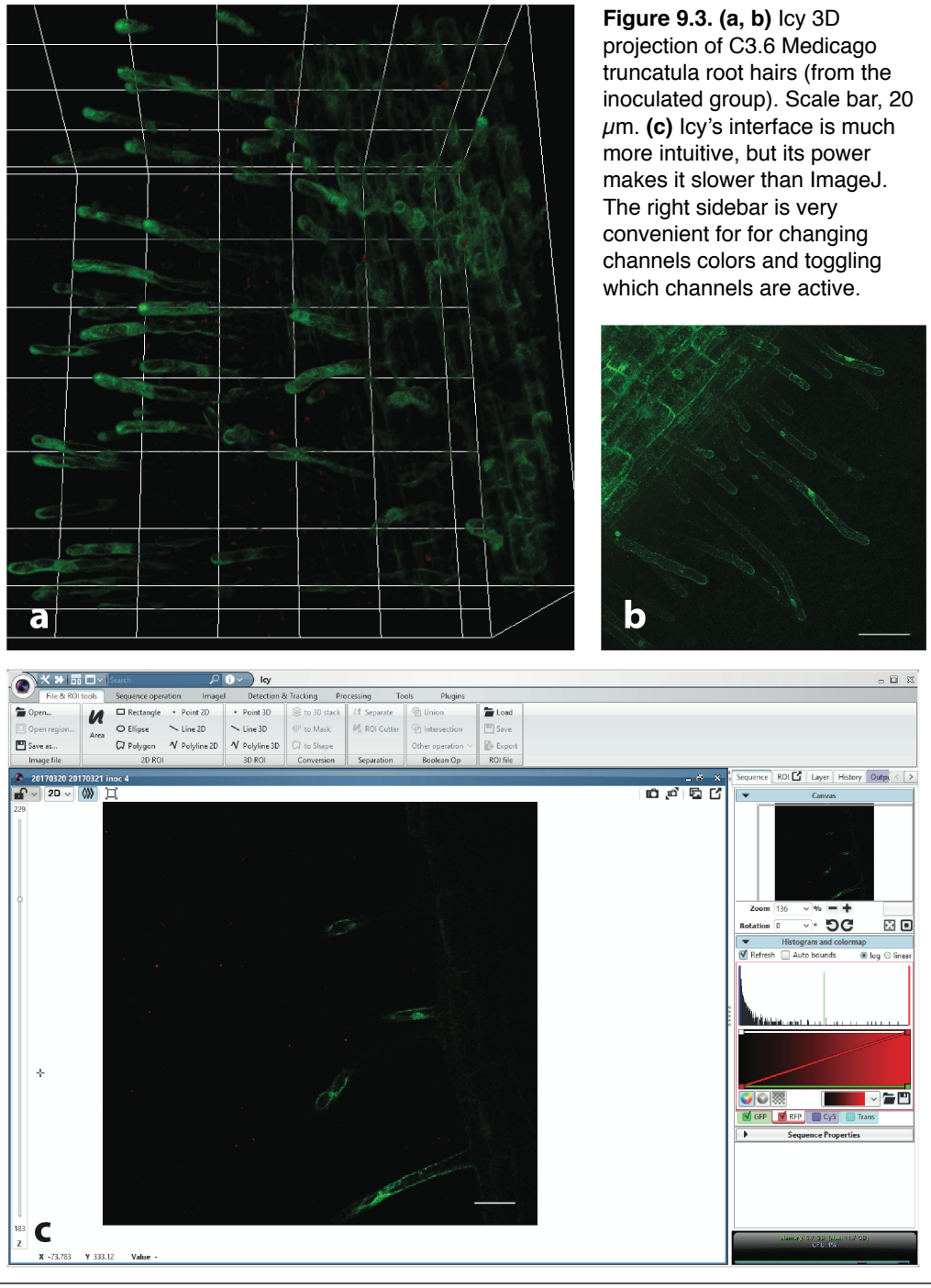

Figure 9.3. (a, b) Icy 3D projection of C3.6 Medicago truncatula root hairs (from the inoculated group). Scale bar, 20 *µ*m. **(c)** Icy's interface is much more intuitive, but its power makes it slower than ImageJ. The right sidebar is very convenient for for changing channels colors and toggling which channels are active.

Figure 10.1. (a, b) YC3.6 *Medicago truncatula* root hairs (from the inoculated group) that have been image processed using a Python script. After the point cloud is generate in Python, it can be viewed using MeshLab.

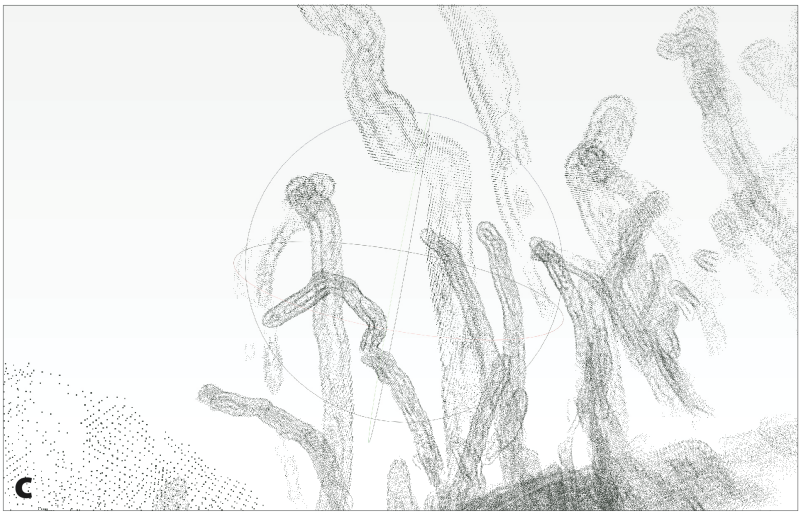

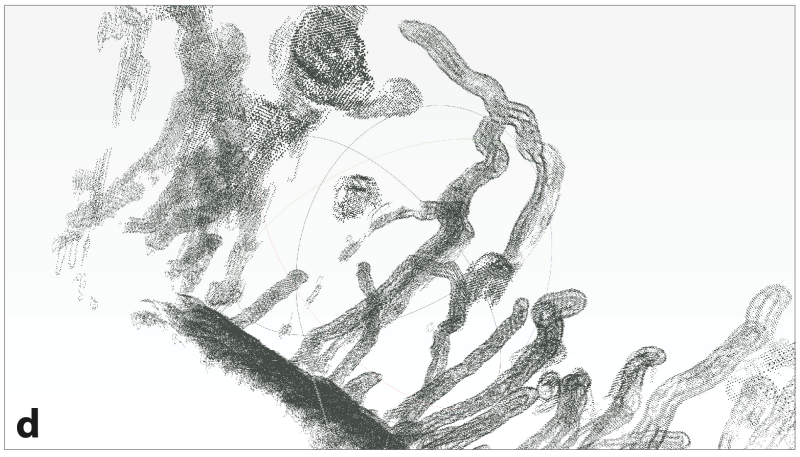

Figure 10.2. (c, d) When viewing in MeshLab, the model can be rotated and explored in ways that are not generally possible in other image analysis software. Although the Python script for processing the image stacks still needs to be fine-tuned, it could be a useful visualization technique.

analysis. Z-stacks with anywhere from 50 – 1000 sections were taken, usually with a z-step (distance between optical sections) between 0.50 and 1.0 µm. Typically the stack was about 500 sections maximum with a z-step of 0.50 µm.

Z-stacks were reconstructed in Icy to show the maximum intensity projection for each stack (Figure 11.1a). This stack was used as a reference during measurements in ImageJ to facilitate root hair identification. Candidates for measurement (those with a visible, recognizable nucleus) were identified

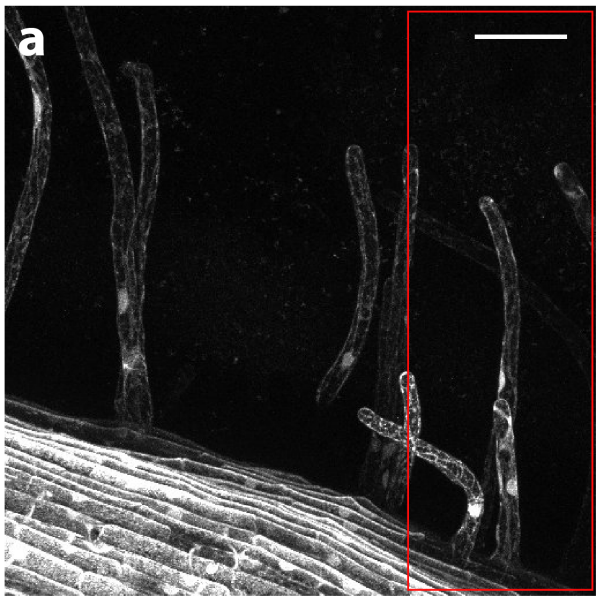

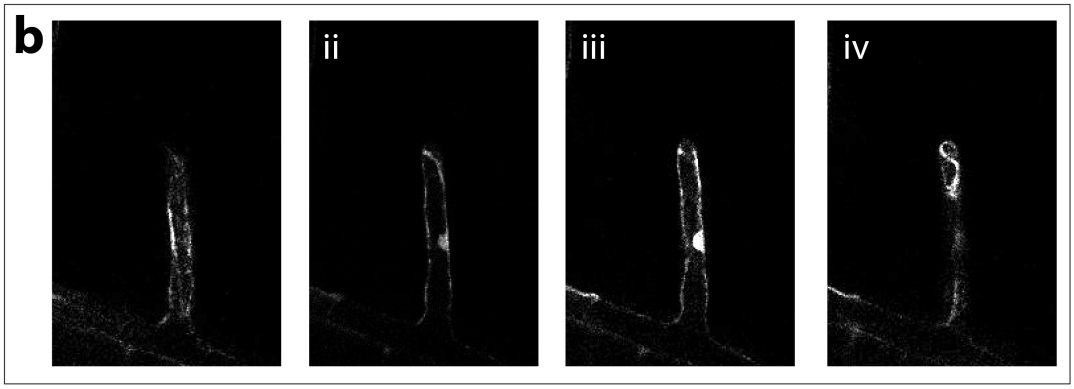

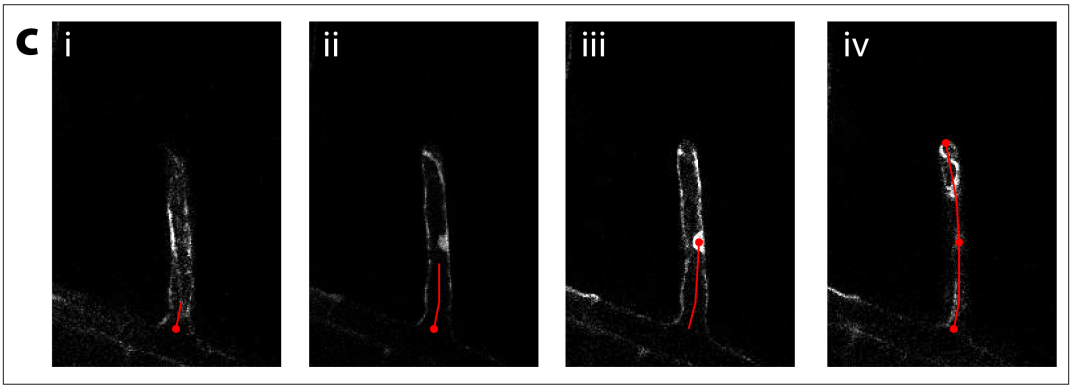

Figure 11.1. The process of identifying a root hair with a visible nucleus that can be measured. The maximum intensity projection **(a)** can be used to see which root hairs are completely captured in the stack. Scale bar, 50 μm. **(b)** This sequence shows different slices of one of the root hairs in this stack. **(c)** This is the same sequence as in **(b)**, but with a red line to show the path traced. The dots show where measurements would be taken. The first measurement point is taken in **(i)**, and then the second point for the nucleus is taken at **(ii)**. Then, the tip distance is taken at **(iii)**. This gives all three measures needed for analysis.

using the maximum intensity projection (Figure 11.1a). On the stack of separated images, the first point was set at the base of the root hair (Figure 11.1c(i)). The “base” was defined at the point at which the tubular portion of the root hair merges with the basal epidermal portion of the cell (Figure 11.1c(i)). The section number at this point was also recorded. Then, I scrolled through the z stack, following the path of the root hair and making additional points using a segmented line, until the nucleus was located (Figure 11.1b-c). Another measurement (length of the segmented line thus far and the section number) was taken for the nucleus (Figure 11.1c(iii)). The nucleus measurement point is at the center of the fluorescent shape marking the nucleus (Figure 11.1c(iii)). Then, I proceeded along the root hair to the tip in the same manner, scrolling through the stack, until I reach the end point at the tip of to root hair (Figure 11.1c(iv)). While measuring through the root hair with the segmented line, I placed the line down the center of the root hair and followed its shape. If a root hair did not have a visible and identifiable nucleus, it was skipped. These measurements were recorded in ImageJ. I measured lengths using ImageJ's Segmented Line tool and recorded the number of sections between the points at the base, nucleus, and tip (Figure 11.1c). Since the spacing between the sections is known, a general z displacement can also be calculated into the lengths (providing an XYZ distance measurement instead of only an XY measurement).

With the measurements I gathered, I compared the following between inoculated and uninoculated seedlings for each day: tip distance, root hair length, and the normalized tip distance to root

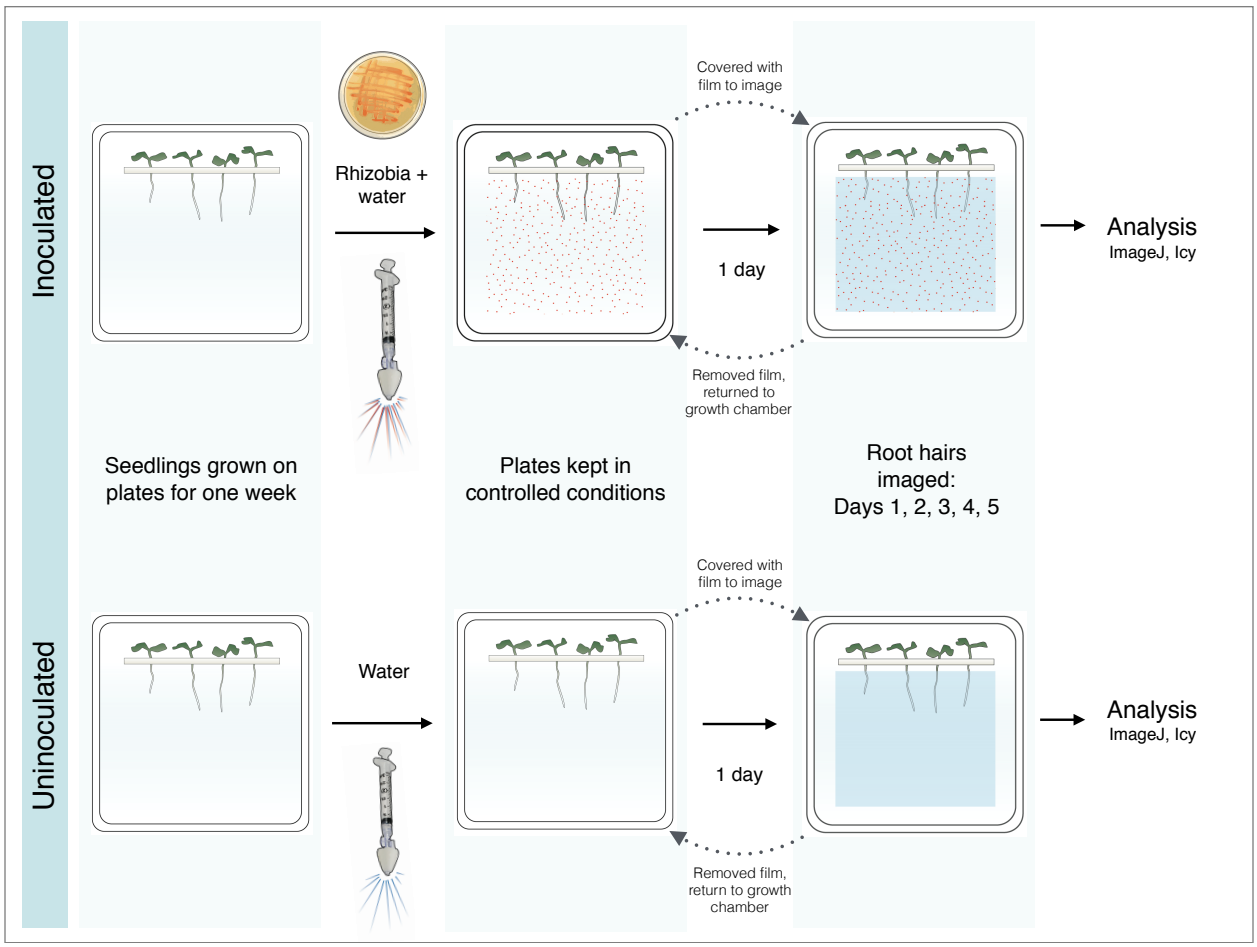

Experimental Design 1. This outline shows the experimental outline for inoculated and uninoculated plants.

hair length. Tip distance is the distance from the nucleus to the tip of the root hair. Root hair length is the total length of the root hair. The normalized tip distance to root hair length is the proportion of the total root hair length that is the distance between the nucleus and the tip.

For days 2 and 3, tip distance was not statistically significantly different between the inoculated and uninoculated treatments ($p>0.05$, Figure 12.2). Days 1, 4, and 5, however, all showed a statistically significant difference between the uninoculated and inoculated treatments ($p < 0.001$ Figure 12.2), with

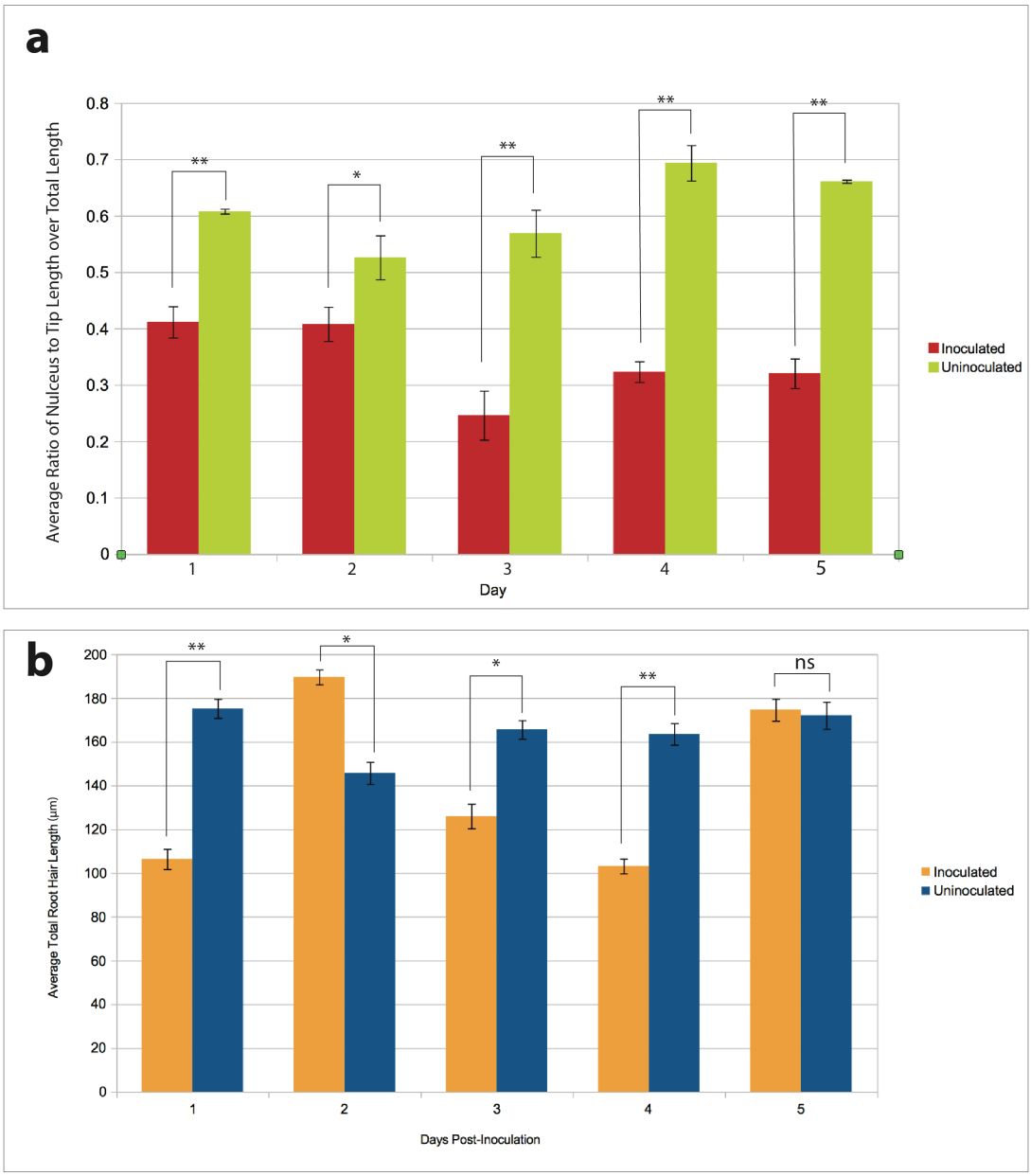

Figure 12.1 a - b. (a) Average ratio of nucleus to tip distance over time (days since post-inoculation). **(b)** Average total root hair length versus days since inoculation between inoculated and uninoculated plants. For **(a)** and **(b)**, ns= not significant, *=p<0.01 and **=p<0.001

the inoculated seedling root hairs having nuclei were significantly closer to the tip compared to the the uninoculated root hair nuclei (Figure 12.2).

According to Sieberer and Emons (2000), a growing root hair has a tip distance of 30±5 µm. When a root hair is stalled and not in a state of tip growth, the nucleus is farther away from the tip (Sieberer and Emons, 2000). The inoculated seedlings on days 1, 4, and 5 have nucleus-to-tip distances of around 30µm (Figure 12.2). This could be interpreted to mean that the root hairs on these days for the inoculated group are experiencing tip growth on these days.

Figure 12.1b shows that root hair length varies both within and between treatments during my time course experiment. Day 2 shows root hair lengths in the inoculated treatment longer than those of the uninoculated group. Uninoculated root hairs were longer on average than inoculated root hairs on day 2 ($p<0.01$), but inoculated root hairs were longer than the uninoculated root hairs on day 1, ($p<0.001$), day 3 ($p<0.01$), and day 5 ($p<0.001$). There was no significant difference between the lengths on day 5 (Figure 12.1b).

The total root hair length differed between the two treatments for days 1, 2, 3, and 4, with the inoculated root hairs being shorter on days 1, 3, and 4, and the uninoculated being shorter on day 2. Nod factors secreted by rhizobia can have effects on plant growth and they are known to have widespread effects on different cell types in the plant (Oldroyd and Downie, 2008). It may be that the observed differences in total length are a result of the effects on root hair development. Since the same zone of the root was imaged every day, it could be that the NFs influence the production of root hairs, causing more young root hairs to be produced. Then, during imaging, these new, shorter root hairs would be in the imaged zone. It should be noted that on day 5 there was no significant difference between the two treatments in terms of total length, even though the distance between the nucleus and root hair tip of inoculated root hairs is similar between day 4 and day 5. In other words, the root hairs for the inoculated

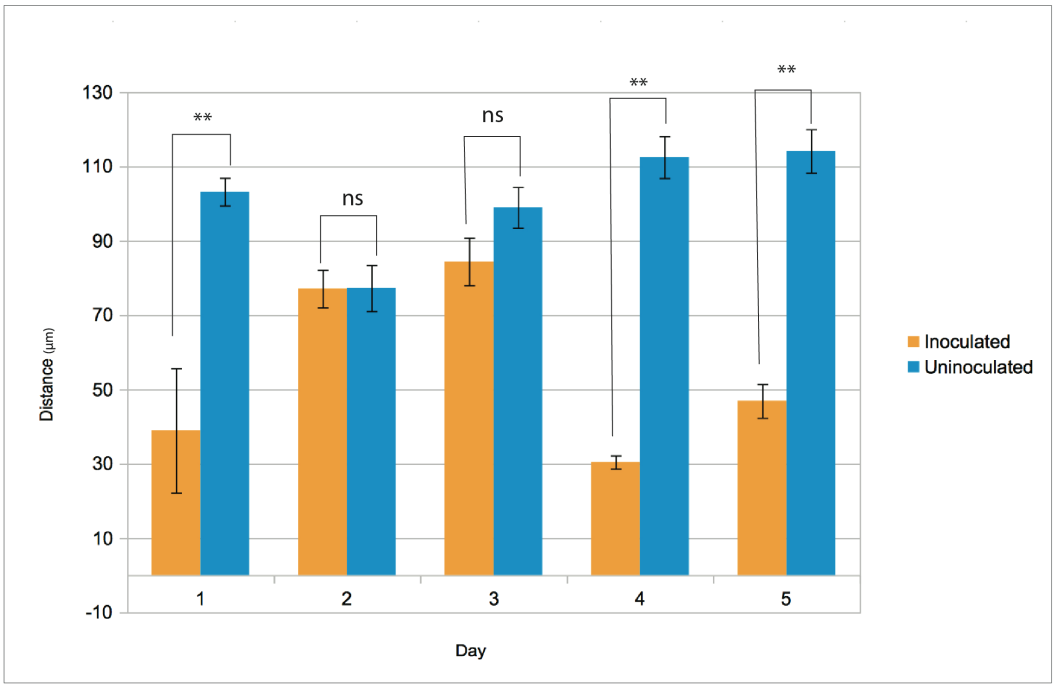

Figure 12.2. Average distance between nucleus and root hair tip between inoculated and uninoculated seedlings. ns= not significant, **=p<0.001

seedlings may have experienced growth due to rhizobial NFs, not just normal developmental growth since it is known that NFs stimulate tip growth (Sieberer and Emons, 2000). On day 5, there is a significant difference between the nucleus-to-tip distances of the inoculated and uninoculated root hairs despite the insignificant difference in the total lengths, suggesting that the inoculated root hairs were experiencing tip growth in preparation for curling (Sieberer and Emons, 2000; Fournier et al. 2008, 2015).

The normalized ratio of nucleus to tip distance over total root hair length (Figure 12.1a) shows that inoculated root hairs, on average per day, had a lower proportion of total root hair length that was the distance between the nucleus and the root hair. Comparison of the inoculated and uninoculated seedlings shows that, on days 1, 3, 4, and 5, there is a statistically significant difference in the ratio of nucleus to tip length to total root hair length between uninoculated plates and inoculated plates (Figure 12.1a). The overall trend of the difference in the ratio of nucleus-to-tip distance over time is a tendency for the inoculated root hairs to exhibit nuclei closer to the tip, while the uninoculated root hairs have nuclei comparatively farther from the tip (Figure 12.1a). It has been observed anecdotally (Fournier et al., 2008, 2015) that root hair nuclei are near the tip during curling, so it is possible that this proportional difference in nucleus-to-tip distance compared to the total root hair length is an early sign of this potential nuclear positioning in inoculated root hairs.

In summary, the data suggest that the root hair nuclei of inoculated *M. truncatula* seedlings are closer to the tips of their respective root hairs than those of uninoculated plants of the same age. Between inoculated and uninoculated plants, the results show that inoculated plants were more likely to have root hair nuclei closer to the tip of the root hair, whereas the the uninoculated plants on average had more nuclei toward the base of the root hair cell, at the epidermis.

DISCUSSION

Experiments

While there have been many anecdotal observations of nuclear activity during rhizobial infection of the legume *M. truncatula*, especially during the extension of the IT, it is not well understood how the nucleus interacts with the rhizobia or infection site prior to root hair curling and subsequent structural changes in the root hair (Fournier et al., 2015). With these preliminary experiments using the YC3.6 line and optimized imaging conditions, the field can begin to contrast these wild type results with the phenotypes of mutants defective for nuclear movement and positioning as well as infection-deficient mutants.

According to the results presented here, it appears as though there is early nuclear movement in response to the presence of rhizobia, especially toward the last three days of the 1-5 day period after inoculation. Nuclei are also likely to be moving in the root hairs during root hair extension at the tip-growing stage. The differences in total root hair lengths between the groups over time is also another interesting area for future investigation. Given that I image root hairs at similar ages on each day, I would have expected that root hair length would remain relatively constant over time. There may be differences in root hair growth depending on rhizobial exposure, or time since rhizobial exposure. Alternatively, the stages may not be as similar as I had thought. The differences between the stages I chose may have resulted in the different total root hair lengths (Figure 12.3). The range of differences in overall length of root hairs for both treatments (Figure 12.3) also suggests that segregating root hairs into size classes would be a useful approach. Here it appears that at days 3 and 4, the root hairs in the imaged region of the root were shorter in the inoculated group than those of the uninoculated group. One possible interpretation of this difference is that there might be variation in the seedling's resource and energy allocation depending on the presence of rhizobia. More studies are needed to compare these details. Additionally, the change in nucleus' distance from the tip may be related to the effect of Nod factors on tip growth in root hairs. At days 2 and 3, the distances between the nuclei and root hair tips of both

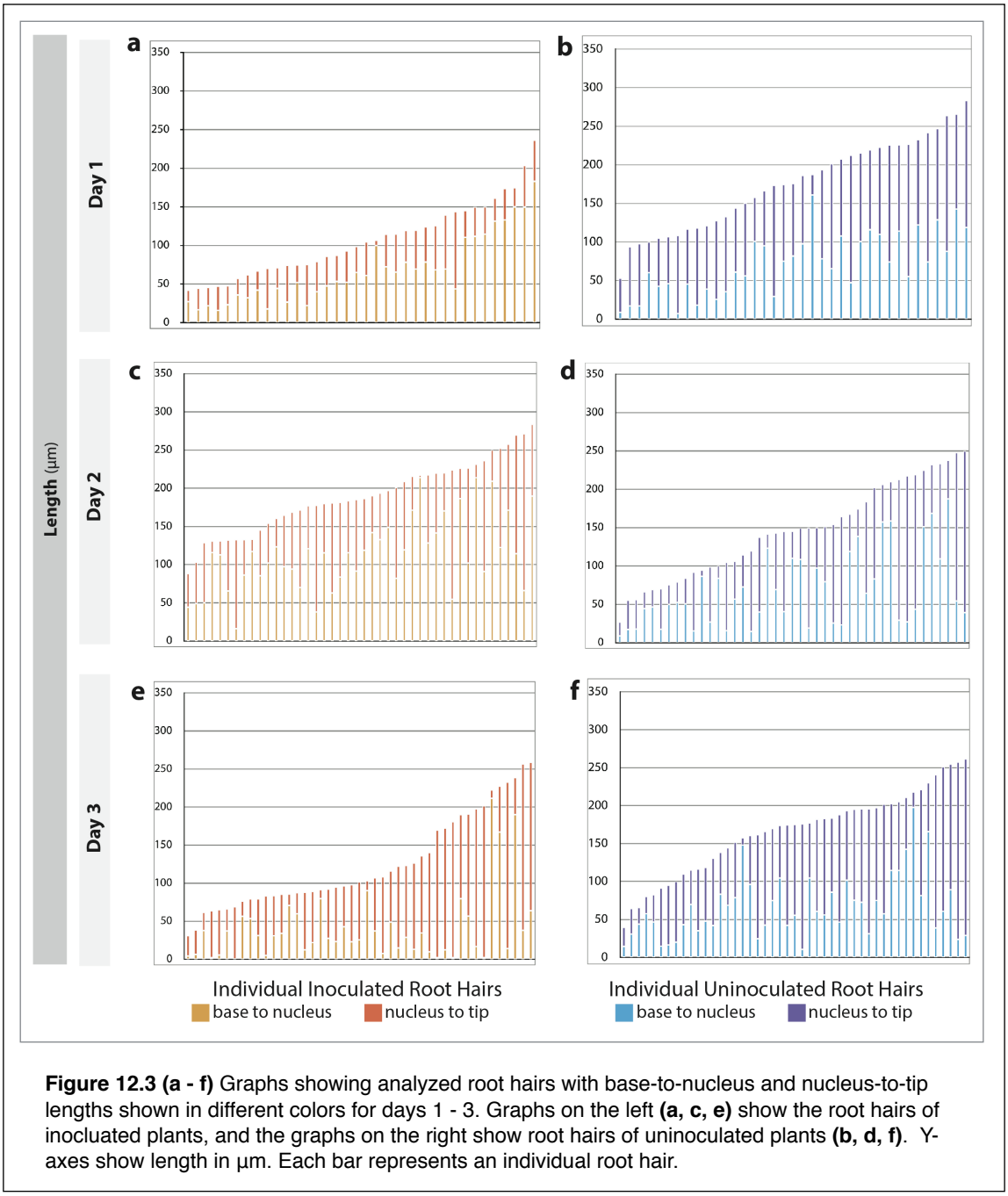

Figure 12.3 (a - f) Graphs showing analyzed root hairs with base-to-nucleus and nucleus-to-tip lengths shown in different colors for days 1 - 3. Graphs on the left **(a, c, e)** show the root hairs of inocluated plants, and the graphs on the right show root hairs of uninoculated plants **(b, d, f)**. Y-axes show length in µm. Each bar represents an individual root hair.

inoculated and uninoculated roots are not significantly different. It is possible that the growth-terminated root hair cells are stimulated to continue tip growth by the presence of the rhizobial Nod factors (Sieberer and Emons, 2009).

Since we expect root hair curling around the 5th day following inoculation, it follows that there would be differences in inoculated and uninoculated root hair nuclear positioning, especially since nuclei near the root hair tip have been noted in previous literature during root hair curling. Further research is needed to correlate this positioning with actual infection events. Figure 12.3 g-j shows the evident differences in nuclear position on days 4 and 5, but more experiments need to be done to focus on days beyond this timeframe. It is not known how many root hairs may respond to the presence of rhizobia or

how many of those responding will actually form ITs or nodules. Longer time course experiments are needed to flesh out the timeline from inoculation for nodule formation.

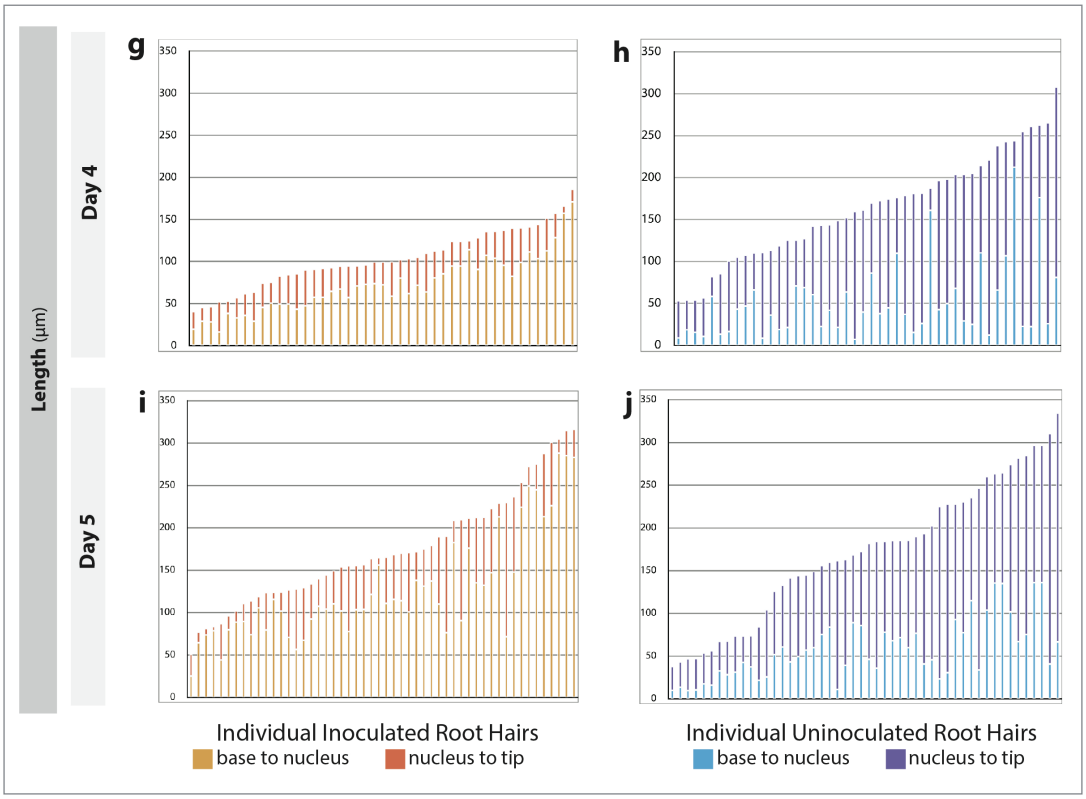

Figure 12.3 (g - j) Graphs showing analyzed root hairs with base-to-nucleus and nucleus-to-tip lengths shown in different colors for days 1 - 3. Graphs on the left (g, i) show the root hairs of inoculated plants, and the graphs on the right show root hairs of uninoculated plants (h, j). Y-axes show length in µm. Each bar represents an individual root hair.

Methods

Visualizations were initially performed in FIJI (ImageJ) using the ClearVolume plugin (Royer et al., 2015). Distances in 3D can be calculated, although the method is somewhat roundabout and requires post calculations. Essentially, mapping a distance on one 2D image is relatively easy, but there are not viable existing plugins to extend this to 3D. However, if the distance between sections is known (it should be retained in the microscopy image metadata), the triangulated distance can be calculated using the Pythagorean theorem. This is not a robust method given that root hairs can move through the Z dimension in rather complex patterns, especially with root hair curling. This method is also very time consuming because the distance line cannot be tracked easily through the Z dimension. The line appears as an overlay on the stack image. I then would have to set a point, move a few sections up or down, set another point, move a few more sections, etc. Even after all of this tedious measuring, the Z component is still only very coarsely estimated.

Further potential analysis of this data can be achieved using Icy. Icy is an open-source (GPLv3)

created by the Quantitative Image Analysis Unit at Institute Pasteur (accessible at www.bioimageanalysis.org). Icy is replete with developer- and user-made plugins that can be utilized for various analyses and visualizations. Like FIJI, it can load confocal data and retains the metadata information that allows for intensity measurements, proper scale, and manipulation of channels. For my purposes, Icy was most useful for determining 3D distances. Not only is Icy's user interface more involved and polished than that of FIJI, it natively downloads with a 3D ROI (Region of Interest) plugin that allows the user to set points while scrolling through the stack, and then the measurement of distance in 3D space is calculated directly in Icy using the 3D Analysis plugins, which also allows for many other measurements to be taken (volume, sphericity, area, flatness, etc.) using the unit calibration from the microscopy file. I did not take measurements of sphericity or circularity of nuclei, but this would be another useful quantification for understanding nuclear dynamics during rhizobial infection.

Although it was not used for quantification or visual aid during quantification, the possibility of the Python script and MeshLab is an exciting one. With this method, a z-stack of 2D sections to be output into an interactive, manipulable 3D model that can be examined and explored more extensively, something other programs don't do as readily. ImageJ and Icy both describe methods for performing a similar operation with their plugins, but I found this difficult to achieve-- they seem to require lots of tweaking with plugins. With the Python script, the images are edited quite rapidly, and the 3D point cloud data is much less intensive in terms of display since it is mathematically drawn in MeshLab. Our initial script and resulting models are currently at a proof-of-concept stage, but the script can be improved to generate point cloud models that can be measured and refined for animations.

Overview

The goal of this project was to determine best practices for *Medicago truncatula* and *Sinorhizobium meliloti* growth and infection, as well as timing of imaging experiments tracking nuclear movement during symbiosis initiations. My results are highly applicable to future studies tracking nuclear movement during this symbiosis, and I have contributed my experience with focus stacking and digital visualizations to provide high-quality resources for those interested in understanding the relationship between these organisms. Furthermore, I have generated the first dataset looking specifically at the positioning of the root hair nucleus in the days leading up to IT formation, including the first stages of legume-rhizobium communication and root hair cellular re-organization.

MATERIALS & METHODS

Plant germination and growth

Medicago truncatula of the R108 ecotype was used for preliminary experiments. After the methods were generally verified for R108 wild type, a stably transformed *Medicago truncatula* line with the fluorescent nuclear marker NLS-YC3.6 (Yellow cameleon 3.6 (Minderer et al., 2011) fused with the SV40 NLS) was used. Final growth conditions are as follows:

Seeds (Figure 13.1) were removed from their pods (Figure 13.2) and scarified using sandpaper, just enough to form an abrasion of the seed coat but not damage the cotyledons or embryo. The seeds are then surface sterilized with 10% bleach (Clorox, NaClO 0.825% NaHCl) for 5-10 minutes (with shaking), rinsed five times with dH20 in the sterile hood, and germinated on plates of 0.5% [w/v] agar in water (Affymetrix, Inc., 10907). These plates were wrapped with Parafilm (Bemis Company, Inc., PM996) to prevent dehydration, wrapped in aluminum foil to block light, and cold treated at 4° C for three days. Then, the seedlings were transferred to a controlled light and temperature growth chamber (20° C, 18 hour day/6 hour night) to germinate. Germination occurred within two to three days following removal from the dark. When cotyledons of the seedlings began to appear green (Figure 13.3), seedlings were

Figure 13.1. *M. truncatula* R108 seeds, prior to being sterilized or scarified. Scale bar, 3 mm.

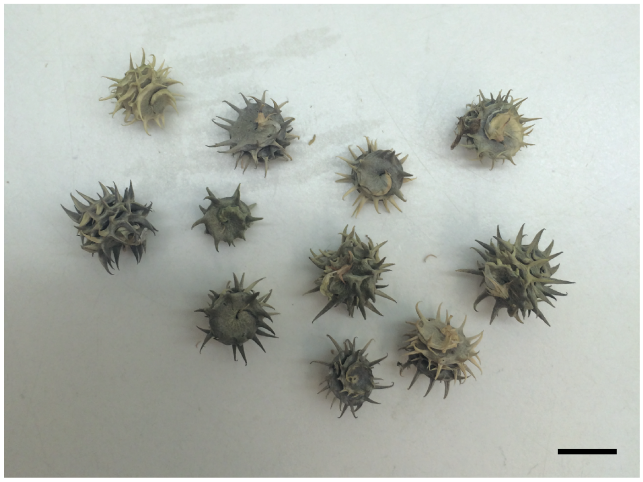

Figure 13.2. *M. truncatula* R108 seed pods. Seed pods were dissected using forceps. Scale bar, 5 mm.

transferred from the germination plates to 12 cm x 12 cm Phytagel-AVG-modFP medium (Fournier et al., 2008; see Media section for details) The seedlings were arranged in a single row at the top of the plate to allow enough space for root growth, with three to four seedlings per plate (Figure 13.4). A strip of filter paper was cut and laid over the row of seedling at the hypocotyl (Figure 5.2) to prevent the seedlings from falling off of the solid medium (Figure 5.1b). Plants were grown vertically in the controlled temperature and light chamber (20° C, 18 hour day/6 hour night) (Figure 5.1a).

Media

The media used is specifically formulated to be deficient in plant-available nitrogen. The Phytagel-AVG-modFP (pH 6) recipe (Fournier et al., 2008) was a modified version of Fahraeus medium (modFP) (Fahraeus, 1957), with an increased concentration of MgSO4 and 0.5% [w/v] Phytagel (Sigma) (Fournier et al., 2008). The recipe is as follows: 0.9mM CaCl2, 3.0 mM MgSO4, 0.7mM KH_2PO_4, 0.8mM $Na_2HPO_4 \cdot 2H_20$, 0.02 Ferric citrate. The medium was supplemented with 50 nM 2-aminoethoxyvinyl Glycine (AVG,

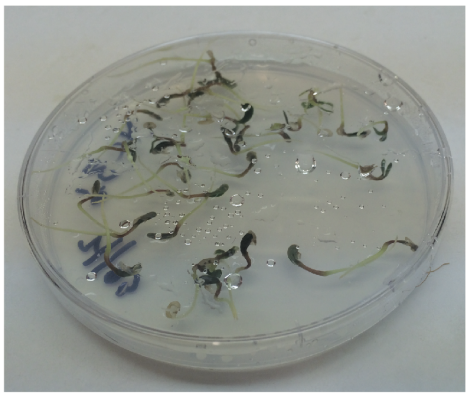

Figure 13.3. *M. truncatula* R108 seedlings with green cotyledons, ready to be plated.

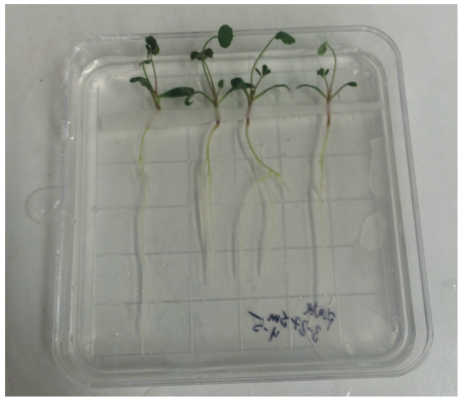

Figure 13.4. *M. truncatula* R108 seedlings on a Phytagel plate with four seedlings and a strip of paper keeping them on the plate.

Sigma, (S)-trans-2-Amino-4-(2-aminoethoxy)-3-butenoic acid hydrochloride, cat. No. A6685) (Fournier et al., 2008; 2015). AVG limits ethylene production, and has been demonstrated that ethylene could inhibit the process of nodulation (Peters and Crist-Estes, 1989; Guinel and Geil, 2002).

Rhizobium complete tryptone-yeast medium (TY) was used to grow *S. meliloti* in liquid culture and on plates. TY liquid medium (pH 7.5) consisted of the following: 0.5% [w/v] tryptone (Fisher, BP1421-2), 0.3% [w/v] yeast extract (Affymetrix, 23547), 0.012 M CaCl2 (Sigma-Aldrich, 223506-500G). For solid TY medium (pH 7.5), 1.5% [w/v] agar (Affymetrix, Inc., 10907). 50 µg/mL streptomycin and 5 µg/mL tetracycline were added to media after sterilization for selection.

Rhizobia growth and inoculation

Sinorhizobium meliloti 2011 dsRed (M. Charpentier) is grown on plates of TY solid media 50 µg/mL streptomycin and 5 µg/mL tetracycline (Figure 1.2). For seedling inoculation, liquid cultures of *S. meliloti* in 5 mL TY media are grown overnight at 28° C with shaking until they are growing in an exponential phase (OD = 0.1). After cultures were grown to this point, aliquots of 1 mL were made in 1.7 mL microcentrifuge tubes. These tubes were centrifuged at 6000 rpm for 1 minute to separate the

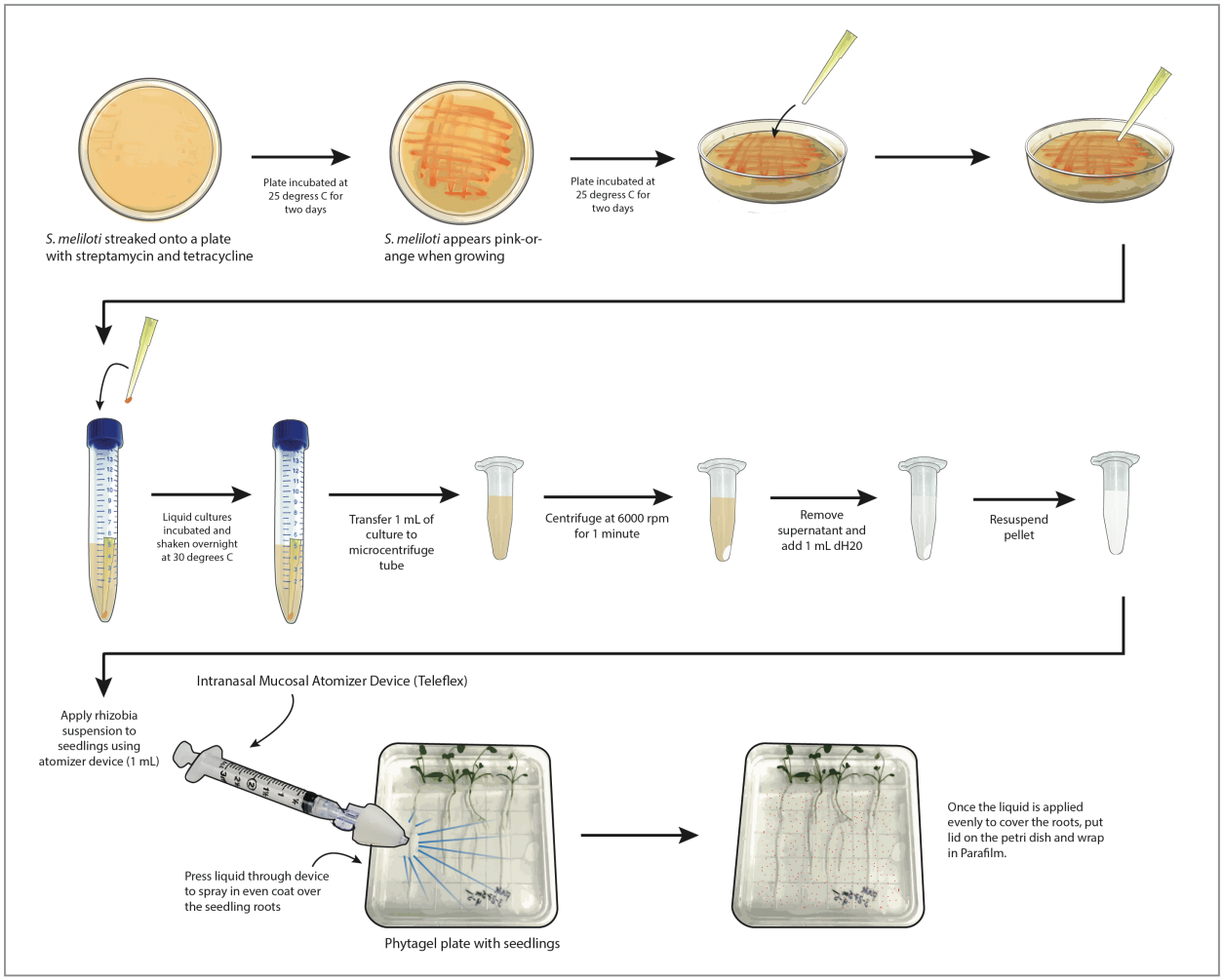

Workflow 1. This outline shows the procedure of culturing *S. meliloti* 2011 dsRed and applying it to plates of *M. truncatula* seedlings.

rhizobia from the TY growth medium. The TY was discarded, rhizobia were resuspended in 1 mL sterile distilled water, and the 1 mL aliquots were then ready to be applied to plates of seedlings. See Workflow 1 for an illustrated guide of this process.

Inoculation procedure

Plants were inoculated with *Sinorhizobium meliloti* 2011 dsRed using an intranasal mucosal atomization (MADs) device (Teleflex, Cat. No. MAD140) for even coverage (Workflow 1, last step). Liquid cultures of *S. meliloti* were prepared as above, and the 1 mL of suspended rhizobia was poured into the syringe of the MADs device. The plunger was then used to slowly press the liquid out. As the liquid exited the MADs device, it was atomized into very small droplets. This allowed the liquid to be widely and consistently distributed throughout the area of the plated seedlings. See Workflow 1 for an illustrated guide of this process.

Imaging conditions

Seedlings were covered on their plates with Lumox film (Sarstedt, Inc., cat. no. 94.6077.317), which is a gas permeable and transparent plastic film. The film has the same refractive index as water and allows direct and repeated confocal microscopy of the seedlings using water-immersion objectives (figure 2.1). Initially the methodology was tested using wild type *Medicago truncatula* from the R108 ecotype. Once the process began to appear relatively stable and reliable, the YC3.6 line was used. At the time of imaging, the Parafilm sealing the Phytagel seedling plates was removed, and the plates were opened so that water could be added and the film could be applied. A thin layer of sterile dH20 was applied to cover the roots (about 1 mL) and then a rectangular piece of film was cut using ethanol-sterilized scissors, The film was carefully laid over the roots only, leaving the cotyledons and other leaves uncovered. These were then imaged using an Eclipse C90i (Nikon) confocal microscope (see below) using either the 4X or 40X objective (see Microscopy section for details). To image using the 40X water immersion objective, a small droplet of water was pipetted onto the surface of the film. The plastic material caused the water to form a bead, which can then adhere to the objective (Figure 2.1).

Suitable root hairs were selected based on overall availability and their zone. Root hairs grow in the region of maturation. In order to keep imaging methodical, the root tip was first located. Then, I navigated up the root until root hairs were visible. Areas of roots hairs were skipped if they were too tangled to be reliably measured or if the root hairs were too long to fit within the frame of the image. The 40x objective generates an image that is 318.5 x 318.5 µm, so the entire length of a root hair had to fit within those dimensions in order to be used. Z-stacks anywhere from 50 – 1000 images were taken, usually with a z-step (distance between optical sections) between 0.50 and 1.0 µm. Typically the stack was about 500 images maximum with a z-step of 0.50 µm.

Microscopy

Fluorescence was analyzed with an Eclipse C90i (Nikon) confocal microscope, equipped with a plan Apochromat VC box H case (numerical aperture 1.4). The objective used for distance measurement assays was the Nikon 40x/0.80W, DIC M/N2, infinity/0 WD 2.0 water immersion objective. Images of the gross morphology of the root (used to scan for areas of visible root hairs) were obtained using the Nikon 4x/0.13, infinity/- WD, 17.2 air objective. GFP fluorescence was imaged with a 488-nm laser. RFP fluorescence was imaged with a 570-nm laser.

Image Analysis

Images were analyzed using ImageJ and OpenOffice Calc. 3D models and projections were generated using ImageJ (and plugins), Icy, and Python scripting with MeshLab. For quantifications, ImageJ was used to take measurements. ImageJ imports metadata regarding the calibrated measurements of the pixels, so all of its outputs are in the desired units (µm). Icy was used to generate a maximum intensity projection during measuring; having a compilation of the stack while analyzing images helps give a frame of reference for following the path of root hairs through the z dimension. A table listing advantages and disadvantages of each was composed s a reference for future applications of these softwares (Table 1).

Comparison of image analysis and visualization software

	Advantages	Disadvantages
NIS Elements AR v. 3.2	- Real-time visualizations are high-quality - 3D projections are easy to generate - Measuring is easily done, with everything exportable in data sheet	- Expensive - Difficult to share protocols or find plugins since the software must be licensed
ImageJ / FIJI 1.51k 1	- Light, easy to use - Open source with lots of well-documented variety plugins & online community - Measurements are easy to take and can be exported as data sheet - Console shows errors	- Menus can be heavily nested - Configuring channels is done in dropdown menus
Icy v. 1.9.1.0	- Accessible and intuitive interface - Open source with a fair amount of documentation - 3D models can be easily generated and manipulated	- Plugins are very specific and geared toward biomedical applications - Not as widely used - Depending on stack size, live viewing of a 3D projection may be slow
Python v. 3.6.1 & MeshLab v. 2016.12	- Potentially useful applications - Possibility to modify the script to achieve desired results rather than relying on other software - Open source	- New and not extensively developed - Learning curve may be an issue for those not familiar with coding / 3D modeling

Table 1. Comparison of explored image analysis and visualization software.

ACKNOWLEDGEMENTS

I would like to sincerely thank the following people for their involvement in my Honors Research Thesis: **Dr. Iris Meier** for being my faculty advisor & thesis committee member, for allowing me to explore and conduct experiments in her lab, and for teaching me to think critically about research; Ph. D. candidate **Anna Newman-Griffis** for assisting with my project, being an incredible mentor over the past three years, and teaching me everything; **Dr. Gregory Booto**n for being one of my thesis committee members, introducing me to molecular genetics & statistics, and for always being so happy to answer questions in & out of the classroom; **Amy Youngs** for being one of my thesis committee members, for supporting my projects, and for encouraging me to explore interdisciplinary work. I extend my deepest appreciation for everything that they have taught me in my undergraduate career.

REFERENCES

Akcay, E., and Roughgarden, J. (2007). Negotiation of mutualism: Rhizobia and legumes. Proc. Bio. Sci. 274:1606, 25-32.

Boisson-Dernier, A., Andriankaja, A., Chabaud, M., Niebel, A., Journet, E. P., Barker, D.G., and de Carvalho-Niebel, F. (2005). MtENOD11 gene activation during rhizobial infection and mycorrhizal arbuscule development requires a common AT-rich-containing regulatory sequence. Mol. Plant Microbe Interact. 18, 1269–1276.

Catoira, R., Timmers, A. C. J., Maillet, F., Galera, C., Penmetsa, R. V., Douglas, C., Denarie, J., and Gough, C. (2001). The HCL gene of *Medicago truncatula* controls Rhizobium-induced root hair curling. Develop. 128, 1507-1518.

Charpentier, M., Sun, J., Van Martins, T., Radhakrishnan, G. V., Findlay, K., Soumpourou, E., Thouin, J., Very, A., Sanders, D., Morris, R. J., and Oldroyd, G. E. D. (2016). Science 352:6289, 1102-1105.

Cignoni, P., Callieri, M., Corsini, M., Dellepiane, M., Ganovelli, F., and Ranzuglia, G. (2008). Meshlab: an open-source mesh processing tool. Eurographics Italian Chapter Conference 2008, 129-136.

de Chaumont, F., et al. (2012). Icy: an open bioimage informatics platform for extended reproducible research. Nature Methods 9, 690-696. http://icy.bioimageanalysis.org

Fahraeus, G. (1957). The infection of clover root hairs by nodule bacteria studied by a simple class slide technique. J. Gen. Microbiol.16, 374-381.

Fournier, J., Teillet, A., Chabaud, M., Ivanov, S., Genre, A., Limpens, E., de Carvalho-Niebel, F., and Barker, D. G. (2015). Remodeling of the infection chamber before infection thread formation reveals a two-step mechanism for rhizobial entry into the host legume root hair. Plant Phys. 167, 1233–1242.

Fournier, J., Timmers, A. C. J., Sieberer, B. J., Jauneau, A., Chabaud, M., and Barker, D. G. (2008). Mechanism of infection thread elongation in root Hairs of *Medicago truncatula* and dynamic interplay with associated rhizobial colonization. Plant Phys. 148, 1985–1995.

Fournier, J., Timmers, A. C. J., Sieberer, B. J., Jauneau, A., Chabaud, M., and Barker, D. G. (2008). Mechanism of infection thread elongation in root Hairs of *Medicago truncatula* and dynamic interplay with associated rhizobial colonization. Plant Phys. 148, 1985–1995.

Gage, D. J. (2002). Analysis of infection thread development using GFP- and dsRed-expressing *Sinorhizobium meliloti*. J Bacteriol., 7042–7046.

Gage, D. J. (2004). Infection and invasion of roots by symbiotic, nitrogen-fixing rhizobia during nodulation of temperate legumes. Microbiol. Mol. Biol. Rev. 68, 280-300.

Genre, A., Chabaud, M., Timmers, T., Bonfante, P., Barker, G. B. (2005). Arbuscular mycorrhizal fungi elicit a novel intracellular apparatus in *Medicago truncatula* root epidermal cells before infection. Plant Cell 17, 3489-3499.

Genre, A., Chabaud, M., Timmers, T., Bonfante, P., Barker, G. B. (2005). Arbuscular mycorrhizal fungi elicit a novel intracellular apparatus in *Medicago truncatula* root epidermal cells before infection. Plant Cell 17, 3489-3499.

Guinel, F. C., Geil, R.D. (2002). A model for the development of the rhizobial and arbuscular mycorrhizal symbioses in legumes and its use to understand the roles of ethylene in the establishment of these two symbioses. Can. J. Bot. 80, 695-720.

Haynes, J.G., Czymmek, K. J., Carlson, C. A., Veereshlingam, H., Dickstein, R., and Sherrier, D. J. (2004). Rapid analysis of legume root nodule development using confocal microscopy. New Phytol. 163, 661–668.

Journet, E. P., El-Gachtouli, N., Vernoud, V., de Billy, F., Pichon, M., Dedieu, A., Arnould, C., Morandi, D., Barker, D.G., and Gianinazzi-Pearson, V. (2001). *Medicago truncatula* ENOD11: a novel RPRP-encoding early nodulin gene expressed during mycorrhization in arbuscule-containing cells. Mol. Plant Microbe Interact. 14, 737–748.

Kitaeva, A. B., Demchenko, K. N., Tikhonovich, I. A., Timmers, A. C. J., and Tsyganov, V. E. (2016). Comparative analysis of the tubulin cytoskeleton organization in nodules of *Medicago truncatula* and Pisum sativum: bacterial release and bacteroid positioning correlate with characteristic microtubule rearrangements. New Phytol. 210, 168-183.

Küster, H., Becker, A., Samac, D., and Tesfaye, M. (2006). Transcriptomics. In: The *Medicago truncatula* handbook. Mathesius, U., Journet, E. P., Sumner, L. W. (eds). ISBN 0-9754303-1-9.

Moirieri, G., Martinez, E. A., Jarynowski, A., Driguez, H., Morris, R., Oldroyd, G. E. D., and Downie, J. A. (2013). Host-specific Nod-factors associated with *Medicago truncatula* nodule infection differentially induce calcium influx and calcium spiking in root hairs. New Phytol. 200, 656-662.

Moran, N. A. (2006). Primer: Symbiosis. Current Biol. 16:20, R866-R871.

Murray, J. D., Reddy Duvvuru Muni, R., Torres-Jerez, I., Tang, Y., Allen, S., Andriankaja, M., Li, G., Laxmi, A., Cheng, X., et al. (2011). Vapyrin, a gene essential for intracellular progression of arbuscular mycorrhizal symbiosis, is also essential for infection by rhizobia in the nodule symbiosis of *Medicago truncatula*. Plant J. 65, 244-252.

Oldroyd, G. E. D. (2013). Speak, friend, and enter: signaling systems that promote beneficial symbiotic associations in plants. Nature Rev. 11, 252-263.

Oldroyd, G. E. D., and Downie, J. A. (2008). Coordinating nodule morphogenesis with rhizobial infection in legumes. Annu. Rev. Plant Biol. 59, 519-546.

Oldroyd, G. E. D., and Downie, J. A. (2008). Coordinating nodule morphogenesis with rhizobial infection in legumes. Annu. Rev. Plant Biol. 59, 519-546.

Parniske, M. (2008). Arbuscular mycorrhiza: the mother of plant root endosymbioses. Nat. Rev. Microbiol. 6, 763-755.

Peiter, E., Sun, J., Heckman, A. B., Venkateshwaran, M., Riely, B. K., Otegui, M. S., Edwards, A., Freshour, G., Hahn, M. G., Cook, D. R., et al. (2007). The *Medicago truncatula* DMI1 protein modulates cytosolic calcium signaling. Plant Phys. 145, 192-203.

Perrine-Walker, F. M., Lartaud, M., Kouchi, H., and Ridge, R. W. (2014). Microtubule array formation during root hair infection thread initiation and elongation in the *Mesorhizobium-Lotus* symbiosis. Protoplasma 251, 1099–1111.

Peters, N. K., and Crist-Estes, D. K. Nodule formation is stimulated by the ethylene inhibitor aminoethoxyvinylglycine. Plant. Phys. 91, 690-693.

Royer, L. A.; Weigert, M. & Günther, U. et al. (2015). ClearVolume: open-source live 3D visualization for light-sheet microscopy. Nature Methods 12(6), 480-481. PMID 26020498 (on Google Scholar).

Schindelin, J., Arganda-Carreras, I., and Frise, E. et al. (2012). Fiji: an open-source platform for biological-image analysis. Nature Methods 9(7): 676-682, PMID 22743772 (on Google Scholar).

Sieberer, B. J., Chabaud, M., Fournier, J., Timmers, A. C. J., and Barker, D. G. (2012). switch in Ca2+ spiking signature is concomitant with endosymbiotic microbe entry into cortical root cells of *Medicago truncatula*. Plant J. 69, 822-830.

Sieberer, B. J., Chabaud, M., Timmers, A. C., Monin, A., Fournier, J., Barker, D. G. (2009). A nuclear-targeted cameleon demonstrates intranuclear Ca2+ spiking in *Medicago truncatula* root hairs in response to rhizobial Nod factors. Plant Phys. 151, 1197-1206.

Sieberer, B., and Emons, A. M. C. (2000). Cytoarchitecture and pattern of cytoplasmic streaming in root hairs of *Medicago truncatula* during development and deformation by nodulation factors. Protoplasma 214, 118–127.

Swanson, S. J., and Gilroy, S. (2013). Imaging changes in cytoplasmic calcium using the yellow chameleon 3.6 biosensor and confocal microscopy. In: Plant Lipid Signaling. Munnik, T., and Heilmann, I. (eds.). ISBN 978-1-62703-401-2 (eBook).

Timmers, A. C. J. (2008). The role of plant cytoskeleton in the interaction between legumes and rhizobia. J Microscopy 231: 2, 247-256.

Timmers, A. C. J., Stuger, R., Schaap, P. J., Van 'T Riet, J., and Raue, H. A. (1999). Nuclear and nucleolar localization of *Sacchromyces cerevisiae* ribosomal proteins S22 and S25. FEBS Lett. 452:3, 335-340.

Troyo-Dieguez, E., Cortes-Jimenez, J. M., Nieto-Garibay, A., Murillo-Amador, B., Valdéz-Cepeda, R. D., and García-Hernández, J. L. (2010). Ecology and adaptation of Legume Crops. Climate Change Mgmt. Of Cool Season Grain Legume Crops, 23-33.

Turgeon, B. G., and Bauer, W. D. (1985) Ultrastructure of infection-thread development during the infection of soybean by *Rhizobium japonicum*. Planta 163, 328-349.

Van Bruaene, N., Joss, G., and van Oostveldt, P. (2004). Reorganization and in vivo dynamics of microtubules during Arabidopsis root hair development. Plant Phys. 136, 3905-3919.

Wais, R. J., Wells, D. H., and Long, S. R. (2002). Analysis of differences between *Sinorhizobium meliloti* 1021 and 2011 strains using the host calcium spiking response. Mol. Plant Microbe Interact. 15, 1245–1252.

Werner, D., and Newton, W. E. (2005). Nitrogen fixation: origins, applications, and research progress. (Netherlands: Springer).